# Stochastic Sea Ice Modeling with the Dynamically Orthogonal Equations

by

Anantha Narayanan Suresh Babu

B.Tech. (Hons.), Indian Institute of Technology Madras (2020)

Submitted to the
Department of Mechanical Engineering
in partial fulfillment of the requirements for the degree of

Master of Science in Mechanical Engineering

at the

Massachusetts Institute of Technology

September 2023



Authored by: Anantha Narayanan Suresh Babu
Department of Mechanical Engineering
August 27, 2023

Certified by: Pierre F.J. Lermusiaux
Professor, Department of Mechanical Engineering
Thesis Supervisor

Accepted by: Nicolas G. Hadjiconstantinou
Chairman, Department Committee on Graduate Theses

**Stochastic Sea Ice Modeling**

**with the Dynamically Orthogonal Equations**

by

Anantha Narayanan Suresh Babu

Submitted to the
Department of Mechanical Engineering
on August 27, 2023, in partial fulfillment of the
requirements for the degree of
Master of Science in Mechanical Engineering

## Abstract

Accurate numerical models are essential to predict the complex evolution of rapidly changing sea ice conditions and study impacts on climate and navigation. However, sea ice models contain uncertainties associated with initial conditions and forcing (wind, ocean), as well as with parameter values, functional forms of the constitutive relations, and state variables themselves, all of which limit predictive capabilities. Due to the multiple types and scales of sea ice and the complex nonlinear mechanics and high dimensionality of differential equations, efficient ocean and sea ice probabilistic modeling, Bayesian inversion, and machine learning are challenging. In this work, we implement a deterministic 2D viscoplastic sea ice solver and derive and implement new sea ice probabilistic models based on the dynamically orthogonal (DO) equations.

We focus on the stochastic two-dimensional sea ice momentum equations with nonlinear viscoplastic constitutive law. We first implement and verify a deterministic 2D viscoplastic sea ice solver. Next, we derive the new stochastic Sea Ice Dynamically Orthogonal equations and develop numerical schemes for their solution. These equations and schemes preserve nonlinearities in the underlying spatiotemporal dynamics and evolve the non-Gaussianity of the statistics. We evaluate and illustrate the new stochastic sea ice modeling and schemes using idealized stochastic test cases. We employ two stochastic test cases with different types of sea ice: ice sheets and frozen ice cover with uncertain initial velocities. We showcase the ability to evolve non-Gaussian statistics and capture complex nonlinear dynamics efficiently. We study the convergence to the physical discretization, and stochastic convergence to the stochastic subspace size and coefficient samples. Finally, we assess and show significant computational and memory efficiency compared to the direct Monte Carlo method.

Thesis Supervisor: Pierre F.J. Lermusiaux
Title: Professor, Department of Mechanical Engineering

# Acknowledgments

First and foremost, I would like to thank my advisor, Prof. Pierre Lermusiaux, for his support, advice, and mentorship over the last two years. Your passion for research is inspiring, and I am very grateful for your help and guidance with all things, both research and non-research related. Thank you for your patience with me and for providing the flexibility to work on various interdisciplinary topics.

I am grateful to Profs. Arockiarajan, Krishnakannan, and Chandramouli from IIT Madras for encouraging and supporting me to pursue graduate studies at MIT.

I extend my gratitude to Pat and Chris for helping me get set up with the MSEAS cluster and for patiently answering all my questions. Thanks to the MSEAS students for being such a wonderful group. A special thank you to Alonso for being my best friend in the lab and for all the help and fun stories, including during my qualifying exams. Wael, Manan, and Aaron, thank you for all the discussions, insights, and guidance with research ideas. I also want to express my appreciation to Abhinav and Corbin as senior students for making me feel welcome in the group. To Aman, the fellow "Madrasian," thank you for putting up with me during my first year. I'm grateful to Aditya, Tony, and Ellery for being such good friends. I would also like to thank Saana, Una, and Lisa for their quick help with administrative processes.

Prof. Lermusiaux and I are grateful to the Office of Naval Research for their partial support under grants N00014-20-1-2023 (MURI ML-SCOPE) and N00014-19-1-2693 (IN-BDA) at the Massachusetts Institute of Technology. We are also thankful to the MIT School of Engineering for supporting the Homer A. Burnell Presidential Fellowship during the first year of my graduate studies.

Finally, I would like to express my gratitude to my wonderful family. Thank you Amma, Appa, Thatha, Annu mama, Sreemathy mami, and all my extended family and elders for your aseervadham, encouragement, and best wishes. Priya, thank you for being my best friend and for always pushing me to be the best.

# Contents

# List of Figures

# List of Tables

# Chapter 1

# Introduction

In recent years, the need for accurate simulation and prediction of rapidly evolving sea ice conditions has become increasingly apparent, and has quickly become one of the "grand challenges of climate science" [49]. Sea ice extent in the Arctic has been drastically reducing since continuous satellite observations began in November 1978 [77]. Satellite data indicates summer ice melting at an increasing rate year after year, with new ice forming at slower rates in the winter to compensate for the losses. There is also growing consensus towards the possibility of an "ice-free" summer in the Arctic sometime in the next half-century, with significant loss in the ice thickness and concentration [89].

Sea ice conditions have a great impact on our oceans, climate, wildlife, and society. The ice layer acts as an important physical barrier and regulates heat, momentum, and water vapor exchange between the ocean and the atmosphere [98]. It reduces the amount of sunlight absorbed by the ocean, and depending on the thickness, acts as an insulator between the air and the ocean [54]. Sea ice decline has various local and global effects on the ocean, weather, and climate [121]. The local effects include an increase in evaporation, moisture, cloud cover, and precipitation, and new variability in ocean flows and mixing. Globally, there is a significant probability for major changes in the ocean circulation patterns with warmer winters in mid-latitude continents [48, 121]. Sea ice also affects local biodiversity. Summer melting along the ice edges releases trapped nutrients into the ocean, which increases the concentra-

tion of phytoplankton and attracts predators such as whales to the ice edge [52, 25]. The rapidly changing sea ice conditions also affect the migratory patterns of land mammals such as polar bears, increasing the frequency of long-distance swimming [91]. There are also major economic and security implications of the changing ice conditions [7]. Decreasing ice extent has led to improved access near the Arctic for oil and gas exploration [4]. Another impact is the possible opening up of the Northern Sea Route (NSR), Northeast Passage (NEP), and Northwest Passage (NWP) for shorter Arctic shipping between Canada, the United States, Northern Europe and Asia [39, 40].

Hence, it is abundantly clear that there is a need to accurately simulate the sea ice velocities, thickness, and concentration, over multiple scales in time and space. However, this is challenging since sea ice exhibits complex nonlinear material behavior and can exist in forms such as pancakes, floes, and sheets, each with vastly different dynamics [107, 24]. At the scales of today's regional models to Earth Systems Models (ESMs), the numerical resolution ranges from about 10 to 100 km, and sea ice is treated as a continuum [45]. Sea ice was first modeled as a viscous fluid, but these models failed to capture the irreversible formations of leads and ridges under tensile and compressive stresses, respectively [38]. This led to a shift to modeling ice as an elastic-plastic material [85]. Hibler further refined this model using an elliptic yield curve and a normal flow rule, coming up with the Viscous-Plastic (VP) constitutive law, which is now used as the predominant model of choice for various ESMs [37, 45]. This choice was motivated by the observation that collections of plastic sea ice floes behave in an averaged viscous behavior at large length- and time-scales [38]. Other simpler models based on the cavitating fluid approximation have been proposed but do not lead to realistic behavior except when averaged wind forcing is used [22].

The VP model was first solved using a modified Euler time step with successive overrelaxation [37]. This method was refined by [124] to include multiple pseudo-timesteps. This led to the widely used standard semi-implicit solver. Another approach proposed by [43, 42] added an additional artificial elastic term to the VP model to create the Elastic-Viscous-Plastic (EVP) model. This allowed for fully ex-

plicit numerical schemes, which weren't possible for the original VP model due to restrictions on the time step to be of the order of seconds for grid resolutions of 10-100 km for numerical stability [74]. However, it was shown that the EVP model could also result in significantly different solutions from the original VP model, due to the usage of smaller viscosities [81, 79]. More recently, fully implicit solvers utilizing the Jacobian-Free Newton-Krylov method have been proposed for modeling sea ice [57] with parallel implementations [80]. This approach leads to more accurate solutions but is not guaranteed to numerically converge, which has led to efforts to improve the convergence of solutions [58, 106, 86, 74]. Other methods for solving differential equations governing sea ice have also been recently proposed based on Lagrangian approaches [95] and using the Least Squares Finite Element Method [104, 105].

Despite advances in numerical models and methods, there is still significant uncertainty in sea ice predictions [49, 122]. As described earlier, current numerical models use various constitutive formulations and heuristic parameters depending on the modeling length scales, time scales, geographical region, and external conditions [84]. There is also uncertainty associated with initial conditions and external forcing from the wind and ocean fields [6, 62, 65]. Quantifying and predicting the uncertainty of sea ice fields, parameters, and models themselves is thus needed. Such stochastic modeling extends deterministic field estimates to stochastic field and probability density estimates. When uncertainties and nonlinear dynamics are significant, the result is richer and more complete as it predicts the different possibilities and likelihoods. This allows Bayesian data assimilation [97, 26], quantitative risk assessment [3, 114], and Bayesian learning of dynamical models [82, 31]. Therefore, developing probabilistic modeling and uncertainty quantification for sea ice is useful but also crucial for various stakeholders including local populations, forecasters, scientists, and policy and decision-makers [41, 110, 5].

Probabilistic modeling of sea ice is an emerging field, with ensemble methods being used to study the sensitivity of numerical models to specific uncertainties [16]. Various studies have compared and contrasted the effect of model rheology [18] on sea ice forecasts [125, 46, 51]. Many studies have focused on parametric sensitivity

analysis for global sea ice models [94, 119, 90, 120] using ensemble-based methods. The quantification of the sensitivity and uncertainty of ice sheet thickness to initial conditions has also been studied [9]. Some works have focused on the impact of uncertainty in parameters and external forcing such as ice cohesion and wind forcing on sea ice forecasts [93, 14].

## 1.1 Present Research

Although these ensemble-based methods have shown promise, they require a large number of expensive Monte Carlo simulations to handle the complex nonlinear sea ice dynamics and non-Gaussian statistics, which can quickly become computationally intractable. The limited ensemble size of these methods reduces the accuracy of tail estimates for risk and extreme event predictions. These prior advances and limitations lead to several key questions that motivate the present research. They include: How do we handle the complex nonlinear viscoplastic mechanics of sea ice in a stochastic context? Can we obtain stochastic formulations that represent the dominant uncertainties in sea ice modeling in a rigorous probabilistic setting? How can we perform efficient, accurate, and adaptive stochastic reduction, providing rich probabilistic sea ice predictions at a much-reduced cost? Considering these challenges and questions, the Dynamically Orthogonal (DO) equations [102, 19, 20] and Dynamical Low-Rank Approximations [50, 12] offer a principled approach for dynamic model-order reduction and uncertainty quantification. These equations preserve the nonlinearity of the underlying partial differential equations (PDEs), providing a powerful tool for uncertainty prediction. They can also be employed with the Gaussian Mixture Model filter (GMM-DO) [108, 109] and allow for Bayesian data assimilation and learning of parameters, states, and even model formulations themselves [82].

In this work, we focus on probabilistic sea ice predictions and develop new stochastic sea ice models and schemes using the Dynamically Orthogonal (DO) equations. We first implement and verify a deterministic 2D viscoplastic sea ice solver. Next, we derive and implement the new stochastic Sea Ice Dynamically Orthogonal equations.

We illustrate and evaluate our new stochastic sea ice modeling and schemes using a set of idealized test cases. We study the convergence to the physical discretization, stochastic subspace size, and coefficient samples, and asses the computational costs. Finally, we showcase the ability to evolve uncertainties and capture nonlinear spatiotemporal dynamics and non-Gaussian statistics efficiently.

## 1.2 Thesis Outline

The thesis is organized as follows:

- *Chapter 2*: Provides an overview of the deterministic and stochastic sea ice equations, and the problem statement.
- *Chapter 3* : Provides the derivation and implementation of the new stochastic Sea Ice-Dynamic Orthogonal (DO) equations.
- *Chapter 4*: Details the results and discussion of application to idealized test cases of sea ice blocks surrounded by the ocean.
- *Chapter 5*: Highlights the summary of the results and possible extensions of the work.

# Chapter 2

# Background and Problem Statement

In this chapter, we describe the deterministic sea ice governing equations. Next, the stochastic sea ice equations are introduced, and the problem statement is posed.

## 2.1 Deterministic Sea Ice Equations

We consider sea ice blocks surrounded by land or ocean in two-dimensional space. Cartesian coordinates are used with $\boldsymbol{x} = (x, y) \in \mathcal{D}$ denoting the spatial coordinates in the horizontal plane with $\hat{\boldsymbol{i}}$, $\hat{\boldsymbol{j}}$, $\hat{\boldsymbol{k}}$ as the Cartesian unit vectors. We are interested in evolving the sea ice velocities $\boldsymbol{u} = u\hat{\boldsymbol{i}} + v\hat{\boldsymbol{j}}$, the height of the sea ice column $h$, and the sea ice concentration or volume fraction $A$ over time $t$ [59, 44, 37]. Figure 2-1 illustrates a generic model domain and sea ice variables and parameters.

Given the large ratio between the horizontal and vertical scales for typical sea ice problems [15], the momentum equations are posed in 2D as follows [37]:

$$\rho h \frac{D\boldsymbol{u}}{Dt} = -\rho h f(\hat{\boldsymbol{k}} \times \boldsymbol{u}) - \tau_{ocean} + \tau_{wind} + \boldsymbol{\nabla} \cdot \boldsymbol{\sigma} - \rho h g \nabla H_d \tag{2.1}$$

where $\rho$ is the density of ice, $f$ is the Coriolis parameter, $\tau_{ocean}$ and $\tau_{wind}$ are ocean drag and wind stress forcings, $\boldsymbol{\sigma}$ is the Cauchy stress (internal stress) of the sea ice which depends on the rheology, and $H_d$ is the sea surface height. The $\frac{D}{Dt}$ term is the total material derivative which accounts for temporal changes and advection.

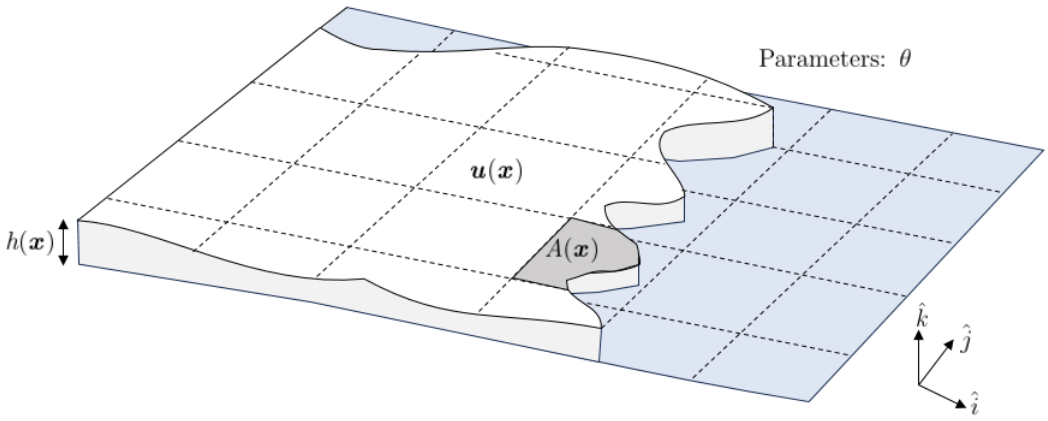


Figure 2-1: Illustration of the model domain and sea ice variables considered in the deterministic setting. The 2D $\boldsymbol{x} = (x, y)$ domain contains sea ice blocks surrounded by land or ocean. We are interested in modeling the sea ice velocities $\boldsymbol{u}(\boldsymbol{x}, t)$, sea ice height $h(\boldsymbol{x}, t)$, and sea ice concentration $A(\boldsymbol{x}, t)$. The set of model parameters are denoted by $\theta$.

However, due to the relatively low velocities of pack ice, the advective terms are orders of magnitude smaller compared to the nonlinear diffusion and forcing [88, 43].

There are many models for the wind and ocean drag forcing. One of then uses an empirical quadratic law with a constant turning angle [85]:

$$\tau_{ocean} = \rho_w C_{dw} |\boldsymbol{u} - \boldsymbol{u_w}| \big( (\boldsymbol{u} - \boldsymbol{u_w}) \cos\theta_w + (\hat{\boldsymbol{k}} \times (\boldsymbol{u} - \boldsymbol{u_w})) \sin\theta_w \big) \tag{2.2}$$

$$\tau_{air} = \rho_a C_{da} |\boldsymbol{u_a}| \big( (\boldsymbol{u_a}) \cos\theta_a + (\hat{\boldsymbol{k}} \times (\boldsymbol{u_a})) \sin\theta_a \big) \tag{2.3}$$

where $\rho_a$ and $\rho_w$ are the densities of air and water respectively, $\boldsymbol{u_a}$ and $\boldsymbol{u_w}$ are wind and ocean velocities (in some cases, they are set to their geostrophic component [57]), $\hat{\boldsymbol{k}}$ is the Cartesian co-ordinate in the vertical direction, $C_{da}$ and $C_{dw}$ are the drag coefficients of wind and water, respectively. It should be noted that in typical problems of interest, the wind velocity is orders of magnitude greater than the sea ice velocity.

While various rheologies have been proposed for modeling sea ice dynamics, the viscoplastic (VP) rheology provided by Hibler [37] is the most widely used in practice

and is summarized below. The internal stress of sea ice is modeled as

$$\sigma_{ij} = 2\eta\dot{\epsilon}_{ij} + (\zeta - \eta)\dot{\epsilon}_{kk}\,\delta_{ij} - \frac{P\delta_{ij}}{2} \tag{2.4}$$

where $P$ is the internal ice strength or pressure, $\dot{\epsilon}$ is the symmetric velocity gradient, and $\zeta$ and $\eta$ are the non-linear bulk and shear viscosities.

Since sea ice is a compressible material, the internal ice strength or pressure $P$ is characterized using an equation of state that depends on the sea ice height $h$ and sea ice concentration $A$ as follows [37]:

$$P = hP^{*}exp[-C(1 - A_{ice})] \tag{2.5}$$

where $C$ and $P^{*}$ are empirical constants (with typical values of $C = 20$ and $P^{*} = 27.5 \times 10^{3} Nm^{-2}$).

To account for the nonlinear viscoplastic behavior of sea ice, Hibler's model related the viscosities to the velocity gradients and to the internal pressure using an elliptical yield curve with a normal flow rule, i.e.,

$$\begin{aligned} \zeta &= \frac{P}{2\Delta} \\ \eta &= \frac{\zeta}{e^2} \end{aligned} \tag{2.6}$$

where $e = 2$ is the principal axis ratio of the elliptic yield curve used in the plastic law and $\Delta$ is a viscosity factor defined as follows,

$$\Delta = \left[(1 + \frac{1}{e^2})(\dot{\epsilon}_{11}^2 + \dot{\epsilon}_{22}^2) + (\frac{4}{e^2})\dot{\epsilon}_{12}^2 + 2(1 - \frac{1}{e^2})(\dot{\epsilon}_{11}\dot{\epsilon}_{22})\right]^{\frac{1}{2}} \tag{2.7}$$

It can be seen that $\lim_{\dot{\epsilon}\to 0}\zeta = \infty$ and $\lim_{\dot{\epsilon}\to 0}\eta = \infty$, hence to prevent numerical blow-up, the viscosities are capped explicitly as follows:

$$\zeta = min\left(\frac{P}{2\Delta}, kP\right) \tag{2.8}$$

where $k = 2.5 \times 10^8$ is a capping parameter [37]. Although this capping prevents singularities, it is not continuously differentiable. Hence, an alternate capping proposed by [57] using a hyperbolic function is used instead,

$$\zeta = kP \tanh\left(\frac{1}{2\Delta k}\right) \tag{2.9}$$

Finally, the continuity equations for sea ice height and sea ice concentration are given by,

$$\frac{\partial A}{\partial t} + \boldsymbol{\nabla} \cdot (A\boldsymbol{u}) = S_a \tag{2.10}$$

$$\frac{\partial h}{\partial t} + \boldsymbol{\nabla} \cdot (h\boldsymbol{u}) = S_h \tag{2.11}$$

where $S_a$ and $S_h$ are forcing terms that incorporate the effects of thermodynamics such as freezing, melting, and redistribution or convergence and divergence of mass that leads to the formation of leads and ridges.

For compact notation, we concatenate all the state variables and denote the resulting vector by

$$\boldsymbol{\psi}(\boldsymbol{x}, t) = \begin{bmatrix} \boldsymbol{u}(\boldsymbol{x}, t) \\ A(\boldsymbol{x}, t) \\ h(\boldsymbol{x}, t) \end{bmatrix} \tag{2.12}$$

where $\boldsymbol{x}$ is the position vector in the 2D domain.

The complete governing partial differential equations (PDEs) are thus

$$\frac{\partial}{\partial t}\boldsymbol{\psi}(\boldsymbol{x}, t) = \begin{bmatrix} \frac{1}{\rho h}\Big( -\rho h f(\hat{\boldsymbol{k}} \times \boldsymbol{u}) - \tau_{ocean} + \tau_{wind} + \boldsymbol{\nabla} \cdot \boldsymbol{\sigma} - \rho h g \nabla H_d \Big) \\ -\boldsymbol{\nabla} \cdot (A\boldsymbol{u}) + S_a \\ -\boldsymbol{\nabla} \cdot (h\boldsymbol{u}) + S_h \end{bmatrix} \tag{2.13}$$

The result 2.13 is a coupled system of stiff PDEs that govern the sea ice dynamics.

This equation can be represented in a compact manner as

$$\frac{\partial}{\partial t}\boldsymbol{\psi}(\boldsymbol{x}, t) = \mathcal{L}[\boldsymbol{\psi}(\boldsymbol{x}, t), \theta] \tag{2.14}$$

where the vector $\theta$ contains all the parameters used in the model equations $\mathcal{L}$.

## 2.2 Stochastic Sea Ice Equations

We now consider the problem of modeling sea ice under uncertainty as a stochastic dynamical system. Such a system can have multiple sources of uncertainty including uncertain initial conditions, uncertain boundary conditions, uncertain forcing, uncertain model parameters, and uncertain model formulations themselves [65, 63, 82, 31]. As described in Chapter 1, all of these types of uncertainties play a role in sea ice forecasts. There is indeed significant uncertainty in the predictions of sea ice models due to unknown initial conditions [6], boundary conditions and external forcing [14, 93], parameters values [92, 120], and competing model formulations [84] and rheologies [125, 46, 51]. Figure 2-2 illustrates a generic model domain with uncertain states and parameters.

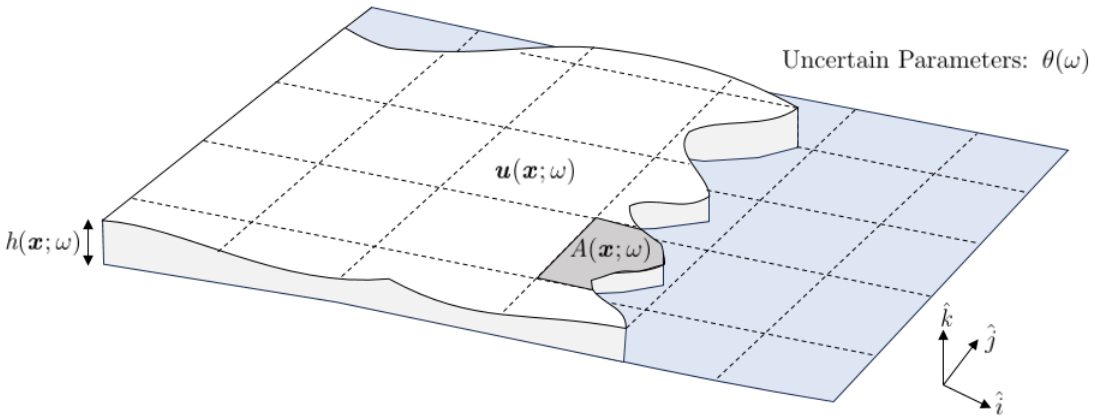


Figure 2-2: Illustration of the model domain and sea ice variables considered in the stochastic setting. The 2D model domain contains uncertain sea ice blocks surrounded by land or ocean. We model the stochastic sea ice velocities $\boldsymbol{u}(\boldsymbol{x}, t; \omega)$, stochastic sea ice height $h(\boldsymbol{x}, t; \omega)$, and stochastic sea ice concentration $A(\boldsymbol{x}, t; \omega)$. The set of uncertain model parameters are denoted by $\theta(\omega)$.

The sea ice state (Eq. 2.12) is then uncertain and represented as a stochastic field $\boldsymbol{\psi}(\boldsymbol{x}, t; \omega)$ where $\omega \in \Xi$, where $\Xi$ is a measurable sample space equipped with an appropriate $\sigma$-algebra $\mathcal{F}$ and probability measure $\mu$. The deterministic PDEs (2.14)

then become a stochastic PDEs (SPDEs) as follows,

$$\frac{\partial}{\partial t}\boldsymbol{\psi}(\boldsymbol{x},t;\omega) = \mathcal{L}[\boldsymbol{\psi}(\boldsymbol{x},t;\omega),\theta(\omega);\omega] \tag{2.15}$$

Modifying equation (2.13) to incorporate uncertainties in the states $\boldsymbol{\psi}(\boldsymbol{x},t;\omega)$ and parameters $\theta(\omega)$, we obtain,

$$\frac{\partial}{\partial t}\boldsymbol{\psi}(\boldsymbol{x},t;\omega) = \begin{bmatrix} -f(\hat{\boldsymbol{k}}\times\boldsymbol{u}(\boldsymbol{x},t;\omega)) - \frac{1}{\rho h(\boldsymbol{x},t;\omega)}\big(\tau_{ocean}(\theta(\omega)) + \tau_{wind}(\theta(\omega)) + \boldsymbol{\nabla}\cdot\boldsymbol{\sigma}(\theta(\omega))\big) - g\nabla H_d \\ -\boldsymbol{\nabla}\cdot(A(\boldsymbol{x},t;\omega)\boldsymbol{u}(\boldsymbol{x},t;\omega)) + S_a(\theta(\omega)) \\ -\boldsymbol{\nabla}\cdot(h(\boldsymbol{x},t;\omega)\boldsymbol{u}(\boldsymbol{x},t;\omega)) + S_h(\theta(\omega)) \end{bmatrix} \tag{2.16}$$

Uncertainties in the model equations could also be incorporated in a similar fashion and have been performed for fluid dynamics and biogeochemical models [82, 31]. We refer to these papers and to [83, 27] for more details.

## 2.3 Problem Statement

In this work, we start by considering the case where the sea ice height and concentrations are known, and the uncertainty is purely in the sea ice velocities and parameters. This is in part because we focus on the specific challenges of sea ice dynamics and we know how to deal with classic advection equations with uncertainties [117, 112, 19]. Solving the momentum equations of sea ice with their nonlinear viscous-plastic behaviors is considered more challenging due to their stiffness than the advection equations for evolving the sea ice height and concentration [106]. We also don't consider the effects of Coriolis forcing and the sea surface tilt [42] as this is also more standard [113, 115]. The first goal is to predict the stochastic sea ice velocity $\boldsymbol{u}(\boldsymbol{x},t;\omega)$ and its probability density distribution in a principled fashion, at higher accuracy and reduced computational cost compared to direct ensemble methods.

Hence, the problem statement for this thesis is to evolve the uncertain sea ice

velocities and their probabilities in space and time, using their governing SPDEs

$$\rho h \frac{\partial}{\partial t}\boldsymbol{u}(\boldsymbol{x}, t; \omega) = -\tau_{ocean}(\theta(\omega)) + \tau_{wind}(\theta(\omega)) + \boldsymbol{\nabla} \cdot \boldsymbol{\sigma}(\theta(\omega)) \tag{2.17}$$

Again, while these SPDEs may appear simple to handle, the divergence of stress tensor term is highly nonlinear from Equations 2.4, 2.6 and 2.7, and requires special treatment. In general, the boundary conditions for Equation 2.17 would be stochastic and we refer to [28] for related schemes.

# Chapter 3

# Methodology

In this chapter, we provide an overview of the Dynamically Orthogonal equations and derive the Dynamically Orthogonal-Sea Ice equations for stochastic sea ice modeling.

## 3.1 Overview of Dynamically Orthogonal Equations

The Dynamically Orthogonal (DO) equations [102, 103, 117] are dynamic instantaneously-optimal reduced-order equations to evolve the dominant uncertainty in high-dimensional stochastic dynamical systems [20, 19, 21]. For a generic stochastic field $\boldsymbol{u}(\boldsymbol{x}, t; \omega)$ governed by a stochastic PDE

$$\frac{\partial \boldsymbol{u}(\boldsymbol{x}, t; \omega)}{\partial t} = \mathcal{L}[\boldsymbol{u}(\boldsymbol{x}, t; \omega); \omega] \tag{3.1}$$

with initial condition

$$\boldsymbol{u}(\boldsymbol{x}, 0; \omega) = \boldsymbol{u}_0(\boldsymbol{x}; \omega) \tag{3.2}$$

where $\boldsymbol{x} \in \mathcal{D}$, $t \in \mathcal{T}$ and $\omega \in \Xi$. The DO decomposition is a dynamic extension of the truncated Karhunen-Loeve decomposition [1, 55, 78]:

$$\boldsymbol{u}(\boldsymbol{x}, t; \omega) = \overline{\boldsymbol{u}}(\boldsymbol{x}, t) + \sum_{i=1}^{n_{s,u}} \tilde{\boldsymbol{u}}_i(\boldsymbol{x}, t) Y_i(t; \omega) \tag{3.3}$$

where $\overline{\boldsymbol{u}}(\boldsymbol{x},t)$ is the mean field, $\tilde{\boldsymbol{u}}_i(\boldsymbol{x},t)$ are orthonormal modes for the stochastic subspace of size $n_{s,u}$, and $Y_i(t;\omega)$ are zero-mean stochastic coefficients. It can be shown that other methods such as polynomial chaos expansion [23, 123] are a subset of DO equations with additional constraints [102]. A significant advantage of the DO equations for stochastic dynamical systems is that both the orthonormal modes as well as the stochastic coefficients are evolved over time.

Next, the DO decomposition (3.3) is inserted into Equation 3.1, and a gauge condition of dynamical orthogonality is enforced on the modes for all times:

$$\left\langle \frac{\partial \tilde{\boldsymbol{u}}_i(\boldsymbol{x},t)}{\partial t}, \tilde{\boldsymbol{u}}_j(\boldsymbol{x},t) \right\rangle = 0 \tag{3.4}$$

$\forall i,j = 1,2,...n_{s,u}$. The mean, mode, and stochastic coefficient evolution equations can then be derived following [101, 102],

$$\frac{\partial \overline{\boldsymbol{u}}(\boldsymbol{x},t)}{\partial t} = \mathbb{E}\big[\mathcal{L}[\boldsymbol{u}(\boldsymbol{x},t;\omega);\omega]\big] \tag{3.5a}$$

$$\frac{\partial \tilde{\boldsymbol{u}}_i(x,t)}{\partial t} = \sum_{j=1}^{n_{s,u}} C^{-1}_{Y_iY_j} \pi_u^{\perp}\big[\mathbb{E}[Y_j(t,\omega)\mathcal{L}[\boldsymbol{u}(x,t;\omega);\omega]]\big], \quad i \in \{1,2,...n_{s,u}\} \tag{3.5b}$$

$$\frac{dY_i(t;\omega)}{dt} = \langle \mathcal{L}[\boldsymbol{u}(\boldsymbol{x},t;\omega);\omega] - \mathbb{E}\big[\mathcal{L}[\boldsymbol{u}(\boldsymbol{x},t;\omega);\omega]\big], \tilde{\boldsymbol{u}}_i(\boldsymbol{x},t)\rangle, \quad i \in \{1,2,...n_{s,u}\} \tag{3.5c}$$

where

$$C_{Y_iY_j} = \mathbb{E}[Y_i(t;\omega)Y_j(t;\omega)] \tag{3.6}$$

and

$$\pi_{\boldsymbol{u}}^{\perp}(\boldsymbol{x}) = \boldsymbol{x} - \pi_{\boldsymbol{u}}(\boldsymbol{x}) = \boldsymbol{x} - \sum_{i=1}^{n_{s,u}} \langle \boldsymbol{x}, \tilde{\boldsymbol{u}}_i(\boldsymbol{x},t)\rangle \tilde{\boldsymbol{u}}_i(\boldsymbol{x},t) \tag{3.7}$$

are the covariance of the coefficients, and the projection operator respectively.

The main advantage of the DO equations is its limited assumption (Equation 3.3) and computational efficiency (Equation 3.5). Up to the truncation to the DO

subspace, the DO equations preserve the nonlinear dynamics and non-Gaussian statistics. The computational efficiency is in part because the equations to be solved are only 1 deterministic PDE for the mean, $n_{s,u}$ deterministic PDEs for the modes, and, if a Monte-Carlo approach is employed for the DO coefficients, $n_r \times n_{s,u}$ stochastic ODEs for the coefficients. This is in comparison to solving $n_r$ PDEs, one for each realization, when a direct ensemble Monte-Carlo method is employed. In typical applications, $n_{s,u} \ll n_r$, which makes the DO equations very efficient in evolving the uncertainties of stochastic PDEs.

## 3.2 Stochastic Dynamically Orthogonal Sea Ice Equations

We follow the approach described above and derive the DO Sea Ice equations for stochastic sea ice modeling. We begin from Equation 2.14 and restrict it to only describe the evolution of the sea ice velocity field $\boldsymbol{u}(\boldsymbol{x})$:

$$\boldsymbol{\psi}(\boldsymbol{x},t) = \begin{bmatrix} u(\boldsymbol{x},t) \\ v(\boldsymbol{x},t) \end{bmatrix} \tag{3.8}$$

where $\boldsymbol{u}(\boldsymbol{x}) = u(\boldsymbol{x})\hat{\boldsymbol{i}} + v(\boldsymbol{x})\hat{\boldsymbol{j}}$. The governing equations are then

$$\begin{aligned} \frac{\partial u}{\partial t} = \frac{1}{\rho h}\Bigg( &- \frac{\partial P}{2\partial x} + \frac{\partial}{\partial x}\left[(\eta+\zeta)\frac{\partial u}{\partial x}\right] + \frac{\partial}{\partial x}\left[(\zeta-\eta)\frac{\partial v}{\partial y}\right] \\ &+ \frac{\partial}{\partial y}\left[\eta\frac{\partial u}{\partial y}\right] + \frac{\partial}{\partial y}\left[\eta\frac{\partial v}{\partial x}\right] + \tau_{wind}\Bigg) \end{aligned} \tag{3.9a}$$

$$\begin{aligned} \frac{\partial v}{\partial t} = \frac{1}{\rho h}\Bigg( &- \frac{\partial P}{2\partial x} + \frac{\partial}{\partial y}\left[(\eta+\zeta)\frac{\partial v}{\partial y}\right] + \frac{\partial}{\partial y}\left[(\zeta-\eta)\frac{\partial u}{\partial x}\right] \\ &+ \frac{\partial}{\partial x}\left[\eta\frac{\partial u}{\partial y}\right] + \frac{\partial}{\partial x}\left[\eta\frac{\partial v}{\partial x}\right] + \tau_{wind}\Bigg) \end{aligned} \tag{3.9b}$$

For compact notation, we define the following:

$$\begin{bmatrix} f_1(u_x, v_x, u_y, v_y, t) \\ f_2(u_x, v_x, u_y, v_y, t) \\ f_3(u_x, v_x, u_y, v_y, t) \\ f_4(u_x, v_x, u_y, v_y, t) \\ f_5(u_x, v_x, u_y, v_y, t) \\ f_6(u_x, v_x, u_y, v_y, t) \end{bmatrix} = \begin{bmatrix} (\eta + \zeta)u_x \\ (\zeta - \eta)v_y \\ \eta u_y \\ \eta v_x \\ (\eta + \zeta)v_y \\ (\zeta - \eta)u_x \end{bmatrix} \tag{3.10}$$

where $x$ and $y$ denote gradients in the x and y directions respectively, i.e, $u_x = \frac{\partial u}{\partial x}$, $u_y = \frac{\partial u}{\partial y}$, $v_x = \frac{\partial v}{\partial x}$ and $v_y = \frac{\partial v}{\partial y}$. Hence,

$$\frac{\partial \boldsymbol{\psi}(\boldsymbol{x}, t)}{\partial t} = \frac{1}{\rho h} \begin{bmatrix} -\frac{\partial P}{2\partial x} + \frac{\partial f_1}{\partial x} + \frac{\partial f_2}{\partial x} + \frac{\partial f_3}{\partial y} + \frac{\partial f_4}{\partial y} + \tau_{wind} + \tau_{ocean} \\ -\frac{\partial P}{2\partial x} + \frac{\partial f_5}{\partial y} + \frac{\partial f_6}{\partial y} + \frac{\partial f_3}{\partial x} + \frac{\partial f_4}{\partial x} + \tau_{wind} + \tau_{ocean} \end{bmatrix} \tag{3.11}$$

Note that in Equation (3.11), the functions $f_1$ and $f_2$ are only present in the $u$-momentum equation while $f_5$ and $f_6$ are only present in the $v$-momentum equation. The functions $f_3$ and $f_4$ appear in both $u$ and $v$ momentum equations but with different spatial gradients ($\frac{\partial}{\partial y}$ in the $u$-momentum and $\frac{\partial}{\partial x}$ in the $v$-momentum).

The DO decomposition is then applied to the stochastic sea ice velocity field $\boldsymbol{\psi}(\boldsymbol{x}, t; \omega)$, using unique stochastic coefficients for the u and v velocities:

$$\boldsymbol{\psi}(\boldsymbol{x}, t; \omega) = \overline{\boldsymbol{\psi}}(\boldsymbol{x}, t) + \sum_{i=1}^{n_{s,\psi}} \tilde{\boldsymbol{\psi}}_i(\boldsymbol{x}, t) Y_i(t; \omega) \tag{3.12}$$

For brevity, we rewrite this decomposition as

$$\boldsymbol{\psi} = \overline{\boldsymbol{\psi}} + \tilde{\boldsymbol{\psi}}_i Y_i \tag{3.13}$$

i.e,

$$u = \overline{u} + \tilde{u}_i Y_i \tag{3.14a}$$

$$v = \overline{v} + \tilde{v}_i Y_i \tag{3.14b}$$

We note that one can employ DO decompositions where the coefficients are not shared for $u$ and $v$. The differences between the approaches are described in [75]. We can also decompose the forcing terms,

$$\tau_{ocean} = \overline{\tau_{ocean}} + \widetilde{\tau}_{oi}\beta_i \tag{3.15a}$$

$$\tau_{wind} = \overline{\tau_{wind}} + \widetilde{\tau}_{wi}\gamma_i \tag{3.15b}$$

where $\beta_i$ and $\widetilde{\tau}_{oi}$ are the stochastic coefficients and modes for the reduced order representation of $\tau_{ocean}$ and $\gamma_i$ and $\widetilde{\tau}_{wi}$ are the stochastic coefficients and modes for the reduced order representation of $\tau_{wind}$.

We now insert the DO decomposition (3.14) into (3.9) to derive the governing DO sea ice equations for the evolution of the mean, the mode, and the stochastic coefficients. However, we need to pay special attention to the nonlinear viscosities in the diffusion terms. For now, we derive the DO evolution equations assuming each of the six nonlinear functions $f$ has a reduced order representation of the form

$$f = \overline{f} + \tilde{f}_i \alpha_i \tag{3.16}$$

where $\alpha_i$ and $\tilde{f}_i$ are the stochastic coefficients and modes for the reduced order representation of $f$. We will describe a local statistical linearization approach to do this later in Section 3.2.1.

Using Equations 3.5, we obtain the evolution equations for the mean, mode, and stochastic coefficients.

$$\frac{\partial \overline{\boldsymbol{\psi}}(\boldsymbol{x},t)}{\partial t} = \begin{bmatrix} -\frac{\partial P}{2\partial x} + \frac{\partial \overline{f}_1}{\partial x} + \frac{\partial \overline{f}_2}{\partial x} + \frac{\partial \overline{f}_3}{\partial y} + \frac{\partial \overline{f}_4}{\partial y} + \overline{\tau_{ocean}} + \overline{\tau_{wind}} \\ -\frac{\partial P}{2\partial y} + \frac{\partial \overline{f}_5}{\partial y} + \frac{\partial \overline{f}_6}{\partial y} + \frac{\partial \overline{f}_3}{\partial x} + \frac{\partial \overline{f}_4}{\partial x} + \overline{\tau_{ocean}} + \overline{\tau_{wind}} \end{bmatrix} \tag{3.17}$$

$$\frac{\partial \tilde{\boldsymbol{\psi}}_i(x,t)}{\partial t} = \sum_{j=1}^{n_{s,\psi}} C^{-1}_{Y_i Y_j} \Bigg( \begin{bmatrix} C_{\alpha_{1_i} Y_j} \frac{\partial \tilde{f}_{1_i}}{\partial x} + C_{\alpha_{2_i} Y_j} \frac{\partial \tilde{f}_{2_i}}{\partial x} + C_{\alpha_{3_i} Y_j} \frac{\partial \tilde{f}_{3_i}}{\partial y} + C_{\alpha_{4_i} Y_j} \frac{\partial \tilde{f}_{4_i}}{\partial y} + C_{\beta_i Y_j} \widetilde{\tau}_{oi} + C_{\gamma_i Y_j} \widetilde{\tau}_{wi} \\ C_{\alpha_{5_i} Y_j} \frac{\partial \tilde{f}_{5_i}}{\partial y} + C_{\alpha_{6_i} Y_j} \frac{\partial \tilde{f}_{6_i}}{\partial y} + C_{\alpha_{3_i} Y_j} \frac{\partial \tilde{f}_{3_i}}{\partial x} + C_{\alpha_{4_i} Y_j} \frac{\partial \tilde{f}_{4_i}}{\partial x} + C_{\beta_i Y_j} \widetilde{\tau}_{oi} + C_{\gamma_i Y_j} \widetilde{\tau}_{wi} \end{bmatrix} \\ - \left\langle \begin{bmatrix} C_{\alpha_{1_i} Y_j} \frac{\partial \tilde{f}_{1_i}}{\partial x} + C_{\alpha_{2_i} Y_j} \frac{\partial \tilde{f}_{2_i}}{\partial x} + C_{\alpha_{3_i} Y_j} \frac{\partial \tilde{f}_{3_i}}{\partial y} + C_{\alpha_{4_i} Y_j} \frac{\partial \tilde{f}_{4_i}}{\partial y} + C_{\beta_i Y_j} \widetilde{\tau}_{oi} + C_{\gamma_i Y_j} \widetilde{\tau}_{wi} \\ C_{\alpha_{5_i} Y_j} \frac{\partial \tilde{f}_{5_i}}{\partial y} + C_{\alpha_{6_i} Y_j} \frac{\partial \tilde{f}_{6_i}}{\partial y} + C_{\alpha_{3_i} Y_j} \frac{\partial \tilde{f}_{3_i}}{\partial x} + C_{\alpha_{4_i} Y_j} \frac{\partial \tilde{f}_{4_i}}{\partial x} + C_{\beta_i Y_j} \widetilde{\tau}_{oi} + C_{\gamma_i Y_j} \widetilde{\tau}_{wi} \end{bmatrix}, \tilde{\boldsymbol{\psi}}_k \right\rangle \tilde{\boldsymbol{\psi}}_k) \Bigg) \tag{3.18}$$

$$\frac{dY_i(t;\omega)}{dt} = \left\langle \begin{bmatrix} \alpha_{1_j} \frac{\partial \tilde{f}_{1_j}}{\partial x} + \alpha_{2_j} \frac{\partial \tilde{f}_{2_j}}{\partial x} + \alpha_{3_j} \frac{\partial \tilde{f}_{3_j}}{\partial y} + \alpha_{4_j} \frac{\partial \tilde{f}_{4_j}}{\partial y} + \beta_j \widetilde{\tau}_{oj} + \gamma_j \widetilde{\tau}_{wj} \\ \alpha_{5_j} \frac{\partial \tilde{f}_{5_j}}{\partial y} + \alpha_{6_j} \frac{\partial \tilde{f}_{6_j}}{\partial y} + \alpha_{3_j} \frac{\tilde{f}_{3_j}}{\partial x} + \alpha_{4_j} \frac{\partial \tilde{f}_{4_j}}{\partial x} + \beta_j \widetilde{\tau}_{oj} + \gamma_j \widetilde{\tau}_{wj} \end{bmatrix}, \tilde{\boldsymbol{\psi}}_i \right\rangle \tag{3.19}$$

where $i \in 1, 2, ...n_{s,\psi}$.

### 3.2.1 Local Statistical Linearization

Since the governing equations (Equation 3.9) contain complex nonlinear viscosities in terms of spatial gradients of velocity, it is not straightforward to obtain their DO expansion. Here, we use a local statistical linearization [72, 112, 31] of the nonlinear terms (e.g., $\frac{\partial}{\partial x}\left[(\eta + \zeta)\frac{\partial u}{\partial x}\right]$ term) around the mean dynamic velocity. This efficiently decomposes the nonlinear terms into their nonlinear mean and sums of stochastic deviations.

For illustration, let us consider the term $f_3(u_x, u_y, v_x, v_y) = \eta \frac{\partial u}{\partial y} = \eta u_y$ where the subscripts $x$ and $y$ again denote gradients in the $x$ and $y$ directions, respectively. We are interested in deriving a decomposition of $f_3$ such that

$$f_3 = \overline{f_3} + \tilde{f}_{3_i} \alpha_{3_i} \tag{3.20}$$

where $\alpha_i$ and $\tilde{f}_{3_i}$ are the stochastic coefficients and modes for the reduced order representation of $f_3$. We perform a local first-order Taylor expansion of $f_3$ around

the mean dynamic velocity gradients to obtain,

$$\begin{aligned} f_3(u_x, v_x, u_y, v_y) =& f_3(\overline{u_x}, \overline{v_x}, \overline{u_y}, \overline{v_y}) + \left.\frac{\partial f_3}{\partial u_x}\right|_{(\overline{u_x},\overline{v_x},\overline{u_y},\overline{v_y})} Y_i \tilde{u_x}_i + \left.\frac{\partial f_3}{\partial v_x}\right|_{(\overline{u_x},\overline{v_x},\overline{u_y},\overline{v_y})} Y_i \tilde{v_x}_i \\ &+ \left.\frac{\partial f_3}{\partial u_y}\right|_{(\overline{u_x},\overline{v_x},\overline{u_y},\overline{v_y})} Y_i \tilde{u_y}_i + \left.\frac{\partial f_3}{\partial v_y}\right|_{(\overline{u_x},\overline{v_x},\overline{u_y},\overline{v_y})} Y_i \tilde{v_y}_i \end{aligned} \tag{3.21}$$

Hence, equating the above two equations yields,

$$\overline{f_3} = f_3(\overline{u_x}, \overline{v_x}, \overline{u_y}, \overline{v_y}) \tag{3.22a}$$

$$\begin{aligned} \tilde{f_3}_i =& \left.\frac{\partial f_3}{\partial u_x}\right|_{(\overline{u_x},\overline{v_x},\overline{u_y},\overline{v_y})} \tilde{u_x}_i + \left.\frac{\partial f_3}{\partial v_x}\right|_{(\overline{u_x},\overline{v_x},\overline{u_y},\overline{v_y})} \tilde{v_x}_i \\ &+ \left.\frac{\partial f_3}{\partial u_y}\right|_{(\overline{u_x},\overline{v_x},\overline{u_y},\overline{v_y})} \tilde{u_y}_i + \left.\frac{\partial f_3}{\partial v_y}\right|_{(\overline{u_x},\overline{v_x},\overline{u_y},\overline{v_y})} \tilde{v_y}_i \end{aligned} \tag{3.22b}$$

$$\alpha_{3_i} = Y_i \tag{3.22c}$$

We note in the above that the terms $\tilde{f_3}_i$ are not orthonormal in general.

Inserting the results from Equation (3.22) (and similar ones for the other nonlinear terms) into Equations (3.18) and (3.19), we obtain

$$\begin{aligned} \frac{\partial \tilde{\boldsymbol{\psi}}_i(x,t)}{\partial t} =& \left( \begin{bmatrix} \frac{\partial \tilde{f_1}_i}{\partial x} + \frac{\partial \tilde{f_2}_i}{\partial x} + \frac{\partial \tilde{f_3}_i}{\partial y} + \frac{\partial \tilde{f_4}_i}{\partial y} \\ \frac{\partial \tilde{f_5}_i}{\partial y} + \frac{\partial \tilde{f_6}_i}{\partial y} + \frac{\partial \tilde{f_3}_i}{\partial x} + \frac{\partial \tilde{f_4}_i}{\partial x} \end{bmatrix} + \sum_{j=1}^{n_{s,\psi}} C^{-1}_{Y_i Y_j} \begin{bmatrix} C_{\beta_i Y_j} \widetilde{\tau_o}_i + C_{\gamma_i Y_j} \widetilde{\tau_w}_i \\ C_{\beta_i Y_j} \widetilde{\tau_o}_i + C_{\gamma_i Y_j} \widetilde{\tau_w}_i \end{bmatrix} \right. \\ &\left. - \left\langle \begin{bmatrix} \frac{\partial \tilde{f_1}_i}{\partial x} + \frac{\partial \tilde{f_2}_i}{\partial x} + \frac{\partial \tilde{f_3}_i}{\partial y} + \frac{\partial \tilde{f_4}_i}{\partial y} \\ \frac{\partial \tilde{f_5}_i}{\partial y} + \frac{\partial \tilde{f_6}_i}{\partial y} + \frac{\partial \tilde{f_3}_i}{\partial x} + \frac{\partial \tilde{f_4}_i}{\partial x} \end{bmatrix} + \sum_{j=1}^{n_{s,\psi}} C^{-1}_{Y_i Y_j} \begin{bmatrix} C_{\beta_i Y_j} \widetilde{\tau_o}_i + C_{\gamma_i Y_j} \widetilde{\tau_w}_i \\ C_{\beta_i Y_j} \widetilde{\tau_o}_i + C_{\gamma_i Y_j} \widetilde{\tau_w}_i \end{bmatrix}, \tilde{\boldsymbol{\psi}}_k \right\rangle \tilde{\boldsymbol{\psi}}_k \right) \end{aligned} \tag{3.23a}$$

$$\frac{dY_i(t;\omega)}{dt} = \left\langle Y_j \begin{bmatrix} \frac{\partial \tilde{f_1}_j}{\partial x} + \frac{\partial \tilde{f_2}_j}{\partial x} + \frac{\partial \tilde{f_3}_j}{\partial y} + \frac{\partial \tilde{f_4}_j}{\partial y} \\ \frac{\partial \tilde{f_5}_j}{\partial y} + \frac{\partial \tilde{f_6}_j}{\partial y} + \frac{\tilde{f_3}_j}{\partial x} + \frac{\partial \tilde{f_4}_j}{\partial x} \end{bmatrix} + \begin{bmatrix} \beta_j \widetilde{\tau_o}_j + \gamma_j \widetilde{\tau_w}_j \\ \beta_j \widetilde{\tau_o}_j + \gamma_j \widetilde{\tau_w}_j \end{bmatrix}, \tilde{\boldsymbol{\psi}}_i \right\rangle \tag{3.23b}$$

where $i \in 1, 2, ...n_{s,\psi}$.

On further simplifications, we derive the final DO mean evolution equations for

the $u$ and $v$ velocities:

$$\rho h \frac{\partial \overline{u}}{\partial t} = -\frac{\partial P}{2\partial x} + \frac{\partial}{\partial x}\left[f_1(\overline{u},\overline{v})\right] + \frac{\partial}{\partial x}\left[f_2(\overline{u},\overline{v})\right] + \frac{\partial}{\partial y}\left[f_3(\overline{u},\overline{v})\right] + \frac{\partial}{\partial y}\left[f_4(\overline{u},\overline{v})\right] + \overline{\tau_{ocean}} + \overline{\tau_{wind}} \tag{3.24a}$$

$$\rho h \frac{\partial \overline{v}}{\partial t} = -\frac{\partial P}{2\partial y} + \frac{\partial}{\partial y}\left[f_5(\overline{u},\overline{v})\right] + \frac{\partial}{\partial y}\left[f_6(\overline{u},\overline{v})\right] + \frac{\partial}{\partial x}\left[f_3(\overline{u},\overline{v})\right] + \frac{\partial}{\partial x}\left[f_4(\overline{u},\overline{v})\right] + \overline{\tau_{ocean}} + \overline{\tau_{wind}} \tag{3.24b}$$

The final DO mode evolution equations for the u and v velocities are:

$$\rho h \frac{\partial \tilde{u}_i}{\partial t} = Q_{u_i} + \sum_{j=1}^{n_{s,\psi}} C^{-1}_{Y_i Y_j}[C_{\beta_i Y_j}\widetilde{\tau}_{oi} + C_{\gamma_i Y_j}\widetilde{\tau}_{wi}] - \left\langle Q_{u_i} + \sum_{j=1}^{n_{s,\psi}} C^{-1}_{Y_i Y_j}[C_{\beta_i Y_j}\widetilde{\tau}_{oi} + C_{\gamma_i Y_j}\widetilde{\tau}_{wi}], \tilde{u}_j \right\rangle \tilde{u}_j \tag{3.25a}$$

$$\rho h \frac{\partial \tilde{v}_i}{\partial t} = Q_{v_i} + \sum_{j=1}^{n_{s,\psi}} C^{-1}_{Y_i Y_j}[C_{\beta_i Y_j}\widetilde{\tau}_{oi} + C_{\gamma_i Y_j}\widetilde{\tau}_{wi}] - \left\langle Q_{v_i} + \sum_{j=1}^{n_{s,\psi}} C^{-1}_{Y_i Y_j}[C_{\beta_i Y_j}\widetilde{\tau}_{oi} + C_{\gamma_i Y_j}\widetilde{\tau}_{wi}], \tilde{v}_j \right\rangle \tilde{v}_j \tag{3.25b}$$

The final DO stochastic coefficient evolution equations for the u and v velocities are:

$$\frac{dY_i(t;\omega)}{dt} = \left\langle Y_j \begin{bmatrix} Q_{u,j} \\ Q_{v,j} \end{bmatrix} + \begin{bmatrix} \beta_j \widetilde{\tau}_{oj} + \gamma_j \widetilde{\tau}_{wj} \\ \beta_j \widetilde{\tau}_{oj} + \gamma_j \widetilde{\tau}_{wj} \end{bmatrix}, \begin{bmatrix} \tilde{u}_i \\ \tilde{v}_i \end{bmatrix} \right\rangle, \quad i \in \{1, 2, ...n_{s,\psi}\} \tag{3.26}$$

$$
\begin{aligned}
\text{where, } Q_{u_i} = & \frac{\partial}{\partial x}\left[\left.\frac{\partial f_1}{\partial u_x}\right|_{(\overline{u},\overline{v})}\tilde{u}_{x_i} + \left.\frac{\partial f_1}{\partial u_y}\right|_{(\overline{u},\overline{v})}\tilde{u}_{y_i} + \left.\frac{\partial f_1}{\partial v_x}\right|_{(\overline{u},\overline{v})}\tilde{v}_{x_i} + \left.\frac{\partial f_1}{\partial v_y}\right|_{(\overline{u},\overline{v})}\tilde{v}_{y_i}\right] + \\
& \frac{\partial}{\partial x}\left[\left.\frac{\partial f_2}{\partial u_x}\right|_{(\overline{u},\overline{v})}\tilde{u}_{x_i} + \left.\frac{\partial f_2}{\partial u_y}\right|_{(\overline{u},\overline{v})}\tilde{u}_{y_i} + \left.\frac{\partial f_2}{\partial v_x}\right|_{(\overline{u},\overline{v})}\tilde{v}_{x_i} + \left.\frac{\partial f_2}{\partial v_y}\right|_{(\overline{u},\overline{v})}\tilde{v}_{y_i}\right] + \\
& \frac{\partial}{\partial y}\left[\left.\frac{\partial f_3}{\partial u_x}\right|_{(\overline{u},\overline{v})}\tilde{u}_{x_i} + \left.\frac{\partial f_3}{\partial u_y}\right|_{(\overline{u},\overline{v})}\tilde{u}_{y_i} + \left.\frac{\partial f_3}{\partial v_x}\right|_{(\overline{u},\overline{v})}\tilde{v}_{x_i} + \left.\frac{\partial f_3}{\partial v_y}\right|_{(\overline{u},\overline{v})}\tilde{v}_{y_i}\right] + \\
& \frac{\partial}{\partial y}\left[\left.\frac{\partial f_4}{\partial u_x}\right|_{(\overline{u},\overline{v})}\tilde{u}_{x_i} + \left.\frac{\partial f_4}{\partial u_y}\right|_{(\overline{u},\overline{v})}\tilde{u}_{y_i} + \left.\frac{\partial f_4}{\partial v_x}\right|_{(\overline{u},\overline{v})}\tilde{v}_{x_i} + \left.\frac{\partial f_4}{\partial v_y}\right|_{(\overline{u},\overline{v})}\tilde{v}_{y_i}\right]
\end{aligned}
\tag{3.27a}
$$

$$
\begin{aligned}
\text{where, } Q_{v_i} = & \frac{\partial}{\partial y}\left[\left.\frac{\partial f_5}{\partial u_x}\right|_{(\overline{u},\overline{v})}\tilde{u}_{x_i} + \left.\frac{\partial f_5}{\partial u_y}\right|_{(\overline{u},\overline{v})}\tilde{u}_{y_i} + \left.\frac{\partial f_5}{\partial v_x}\right|_{(\overline{u},\overline{v})}\tilde{v}_{x_i} + \left.\frac{\partial f_5}{\partial v_y}\right|_{(\overline{u},\overline{v})}\tilde{v}_{y_i}\right] + \\
& \frac{\partial}{\partial y}\left[\left.\frac{\partial f_6}{\partial u_x}\right|_{(\overline{u},\overline{v})}\tilde{u}_{x_i} + \left.\frac{\partial f_6}{\partial u_y}\right|_{(\overline{u},\overline{v})}\tilde{u}_{y_i} + \left.\frac{\partial f_6}{\partial v_x}\right|_{(\overline{u},\overline{v})}\tilde{v}_{x_i} + \left.\frac{\partial f_6}{\partial v_y}\right|_{(\overline{u},\overline{v})}\tilde{v}_{y_i}\right] + \\
& \frac{\partial}{\partial x}\left[\left.\frac{\partial f_3}{\partial u_x}\right|_{(\overline{u},\overline{v})}\tilde{u}_{x_i} + \left.\frac{\partial f_3}{\partial u_y}\right|_{(\overline{u},\overline{v})}\tilde{u}_{y_i} + \left.\frac{\partial f_3}{\partial v_x}\right|_{(\overline{u},\overline{v})}\tilde{v}_{x_i} + \left.\frac{\partial f_3}{\partial v_y}\right|_{(\overline{u},\overline{v})}\tilde{v}_{y_i}\right] + \\
& \frac{\partial}{\partial x}\left[\left.\frac{\partial f_4}{\partial u_x}\right|_{(\overline{u},\overline{v})}\tilde{u}_{x_i} + \left.\frac{\partial f_4}{\partial u_y}\right|_{(\overline{u},\overline{v})}\tilde{u}_{y_i} + \left.\frac{\partial f_4}{\partial v_x}\right|_{(\overline{u},\overline{v})}\tilde{v}_{x_i} + \left.\frac{\partial f_4}{\partial v_y}\right|_{(\overline{u},\overline{v})}\tilde{v}_{y_i}\right]
\end{aligned}
\tag{3.27b}
$$

## 3.3 Numerical Schemes

We now describe the schemes for solving the stochastic DO Sea Ice mean, mode, and coefficient equations. We use the MIT-MSEAS 2.29 finite-volume (FV) framework with staggered grids to solve the PDEs [69, 116]. Using staggered grids leads to easy interpolation of the scalar variables such as ice strength $P$, and nonlinear viscosities, $\zeta, \eta$, to the velocity grids when required [8].

### 3.3.1 Initial Conditions

The initial probability distribution of sea ice fields, or initial stochastic sea ice conditions, should be set according to the dominant initial uncertainties. If the initial probability distribution of the sea ice state variable fields is Gaussian, the dominant initial DO modes are the dominant eigenvectors of the initial covariance matrix. If it is a Gaussian Mixture Model (GMM), dominant modes can be selected based on the dominant eigenvectors of the covariance matrices of each GMM component in accordance with their respective weights. For more on initialization for DO equations, we refer to [64, 61, 103, 108, 109, 115, 27, 76, 75, 31].

One can also generate an ensemble of $n_r$ Monte Carlo initial conditions according to the initial (complex) probability distribution and this is what we employ to initialize the examples provided in Section 4.2 for DO sea ice momentum equations. The mean of these ensembles is then set as the initial condition for the DO mean evolution equation. The DO mode and coefficient initial conditions are obtained from the SVD of the matrix of mean-removed realizations $M$ as follows:

$$M = USV^T \tag{3.28a}$$

$$Y(t=0;\omega) = VS^T \tag{3.28b}$$

$$\tilde{\psi}(\boldsymbol{x}, t=0) = U \tag{3.28c}$$

### 3.3.2 Spatial Discretization

We use a staggered grid, with separate grids for the $u$ and $v$ velocities and the scalar fields such as ice strength and nonlinear viscosities. This decouples the $u$ and $v$ momentum, which aids the efficiency of the numerical solution [124]. A second-order central difference scheme is used for the discretization of all the gradient operators.

The discretization used for the $u$-momentum equations (Fig. 3-1) is

$$\frac{\partial}{\partial x}\left[(\eta+\zeta)\frac{\partial u}{\partial x}\right] = \frac{1}{\Delta x}\left(\left[(\eta+\zeta)\frac{\partial u}{\partial x}\right]_e - \left[(\eta+\zeta)\frac{\partial u}{\partial x}\right]_w\right) \tag{3.29a}$$

$$\frac{\partial}{\partial x}\left[(\zeta-\eta)\frac{\partial v}{\partial y}\right] = \frac{1}{\Delta x}\left(\left[(\zeta-\eta)\frac{\partial v}{\partial y}\right]_e - \left[(\zeta-\eta)\frac{\partial v}{\partial y}\right]_w\right) \tag{3.29b}$$

$$\frac{\partial}{\partial y}\left[(\eta)\frac{\partial v}{\partial x}\right] = \frac{1}{\Delta y}\left(\left[(\eta)\frac{\partial v}{\partial x}\right]_n - \left[(\eta)\frac{\partial v}{\partial x}\right]_s\right) \tag{3.29c}$$

$$\frac{\partial}{\partial y}\left[(\eta)\frac{\partial u}{\partial y}\right] = \frac{1}{\Delta y}\left(\left[(\eta)\frac{\partial u}{\partial y}\right]_n - \left[(\eta)\frac{\partial u}{\partial y}\right]_s\right) \tag{3.29d}$$

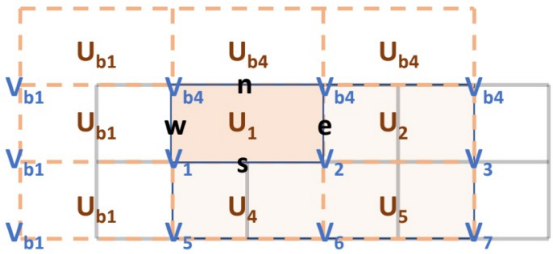


Figure 3-1: Horizontal spatial discretization: $u$-grid cell near the boundary with its associated $n$, $s$, $e$ and $w$ faces.

The discretization used for the $v$-momentum equations (Fig. 3-2) is

$$\frac{\partial}{\partial y}\left[(\eta+\zeta)\frac{\partial v}{\partial y}\right] = \frac{1}{\Delta y}\left(\left[(\eta+\zeta)\frac{\partial v}{\partial y}\right]_n - \left[(\eta+\zeta)\frac{\partial v}{\partial y}\right]_s\right) \tag{3.30a}$$

$$\frac{\partial}{\partial y}\left[(\zeta-\eta)\frac{\partial u}{\partial x}\right] = \frac{1}{\Delta y}\left(\left[(\zeta-\eta)\frac{\partial u}{\partial x}\right]_n - \left[(\zeta-\eta)\frac{\partial u}{\partial x}\right]_s\right) \tag{3.30b}$$

$$\frac{\partial}{\partial x}\left[(\eta)\frac{\partial u}{\partial y}\right] = \frac{1}{\Delta x}\left(\left[(\eta)\frac{\partial u}{\partial y}\right]_e - \left[(\eta)\frac{\partial u}{\partial y}\right]_w\right) \tag{3.30c}$$

$$\frac{\partial}{\partial x}\left[(\eta)\frac{\partial v}{\partial x}\right] = \frac{1}{\Delta x}\left(\left[(\eta)\frac{\partial v}{\partial x}\right]_e - \left[(\eta)\frac{\partial v}{\partial x}\right]_w\right) \tag{3.30d}$$

For the above discrete momentum PDEs, the discrete state variables are the values of $u$ and $v$ at the center of the finite-volume cells. For each physical variable $u$ and $v$, we have $n_{\boldsymbol{x}}$ cells. In what follows, we denote the total number of discrete state variables as $n_{d,\psi}$ which is here equal to $2 \times n_{\boldsymbol{x}}$.

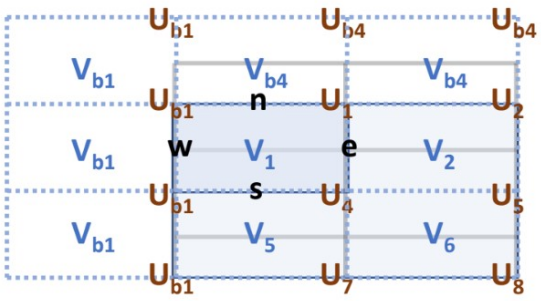


Figure 3-2: Horizontal spatial discretization: $v$-grid cell near the boundary with its associated $n$, $s$, $e$ and $w$ faces.

### 3.3.3 Boundary Conditions

In this thesis, since we only deal with boundary conditions that are deterministic and linear, the mean equation has the same boundary conditions as the realizations. The mode equations have the same type of boundary conditions as the realizations, but with zero values. The coefficient equations do not need boundary conditions since they are just stochastic ODEs. More details on handling stochastic boundary conditions can be found in [28, 27].

Special care must be taken when evaluating the boundary values for scalar variables such as the nonlinear viscosities since the boundary conditions for the problem are only specified for the velocities. This could lead to incompatible boundary values between the viscosities and velocities which are related by Equation (2.6). Some approaches to overcome this issue include utilizing first-order Taylor approximations [56] or splitting the spatial discretization [106]. In this work, we use a second-order Taylor approximation with ghost cells to preserve the spatial convergence.

### 3.3.4 Time Marching

Time integration for the mean equation (3.24) is similar to that of evolving the deterministic sea ice equations. We use the semi-implicit method proposed by [124] where a modified Euler time-step is used. The key advantage of this approach is that the $u$-velocities are treated implicitly, while the $v$-velocities explicitly when solving the $u$-momentum equation, and the $v$-velocities are treated implicitly, and the $u$-velocities

explicitly when solving the $v$-momentum equation.

To integrate the stochastic DO modes using equation (3.25), the nonlinear terms are treated explicitly, and linear terms are treated implicitly. We developed a semi-implicit modified Euler time-step procedure similar to that of the mean equations and this is what we employ in our examples.

Finally, for the stochastic ODEs (3.26), we use an implicit BDF2 (Backward Differentiation Formula) scheme to integrate all the coefficients using a direct Monte Carlo method. This is usually very efficient since there are only $n_{s,\psi}$ scalar ODEs and we have $n_r \gg n_{s,\psi}$ and $n_{d,\psi} \gg n_{s,\psi}$.

Additional details and studies on numerical schemes for the DO equations can be found in [117, 19, 112, 75, 12, 13, 10].

# Chapter 4

# Applications and Discussions

In this section, we implement and validate the deterministic sea ice solver, and study the convergence to spatial discretization. Next, test cases are devised for the stochastic sea ice models with uncertainty in initial conditions and the DO-Sea Ice equations and schemes are tested. We perform convergence analysis to the stochastic subspace size, and coefficient samples, and assess the computational costs.

## 4.1 Deterministic Test Case

The 2D deterministic sea ice solver is implemented within the MSEAS finite volume framework [69, 116]. We also verified the accuracy of the solver using unit tests and the method of manufactured solutions (results not shown here) [96].

The solver is validated using the test case provided in [43]. The deterministic test case is that of a large ice sheet surrounded by land. A constant forcing in space and time acts on the domain, $\tau = 9 \times 10^{-3}\, kg\, m\, s^{-2}$. The total size of the domain is 127 km $\times$ 127 km. A spatial grid resolution of 1.27 km $\times$ 1.27 km is used. The concentration of the ice sheet is set to be 0.9. An implicit time step of $\Delta t$=6 hours is used. The other material parameters used for the test case are the same as those in [43] and are summarized in Table 4.1. Fig. 4-1 shows the $u$ velocity field for this test case, and Fig. 4-2 shows the corresponding nonlinear viscosities. We can see that the viscosities range from $10^{-8}$ to $10^{15}$, which makes stochastic sea ice modeling especially

challenging.

*Spatial convergence analysis.* Next, we perform a spatial convergence study by reducing the grid size, i.e, by increasing the number of finite volume cells. The results of this study are shown in Fig. 4-3. We only use interior points for the convergence study to minimize boundary effects on the rate of convergence. We observe second order spatial convergence, which is expected since we use a second-order central difference scheme for the spatial discretization (Section 3.3.2).

| Parameter | Values | | |
|---|---|---|---|
| | Deterministic | Stochastic # 1 | Stochastic # 2 |
| Domain | 127 km × 127 km | 600 km × 600 km | 600 km × 600 km |
| Spatial resolution | 1.27 km × 1.27 km | 5 km × 5 km | 5 km × 5 km |
| Implicit time step | 6 hours | 0.5 hours | 0.5 hours |
| Sea ice concentration | 0.9 | 0.9 | 0.9, 0.65 |
| Ellipse axis ratio (e) | 2 | 2 | 2 |
| Density of sea ice $(\rho)(kgm^{-3})$ | 910 | 910 | 910 |
| P* $(Nm^{-2})$ | 27.5 $\times 10^3$ | 27.5 $\times 10^3$ | 27.5 $\times 10^3$ |
| C | 20 | 20 | 20 |
| Height of thin ice (h) (cm) | 10 | 10 | 10 |
| Height of thick ice (H) (cm) | 60 | 60 | 60 |
| Viscosity capping (k) | 2.5 $\times 10^8$ | 2.5 $\times 10^8$ | 2.5 $\times 10^8$ |

Table 4.1: Summary of the parameter values used for the deterministic and stochastic test cases. Values used are similar to those in [43] and [106]

## 4.2 Idealized Stochastic Test Cases

Now that we have a validated deterministic sea ice solver, we illustrate and evaluate our new stochastic sea ice modeling and schemes using a set of idealized test cases with initial velocity uncertainties. The uncertainty in initial velocities is of the form

$$\boldsymbol{u}(\boldsymbol{x}, t = 0, \omega) = \boldsymbol{u}_{max}(\omega) \exp\left\{ \frac{-(\boldsymbol{x} - \boldsymbol{x}^*(\omega))^2}{L^2} \right\} \tag{4.1}$$

where $u_{max}$ is the amplitude of the initial velocity, uniformly distributed between 2-10 cm/hr, and $\boldsymbol{x}^*$ the location of the maximum initial velocity, also uniformly distributed spatially across the 2D domain. This initialization is illustrated in Fig. 4-4 by three

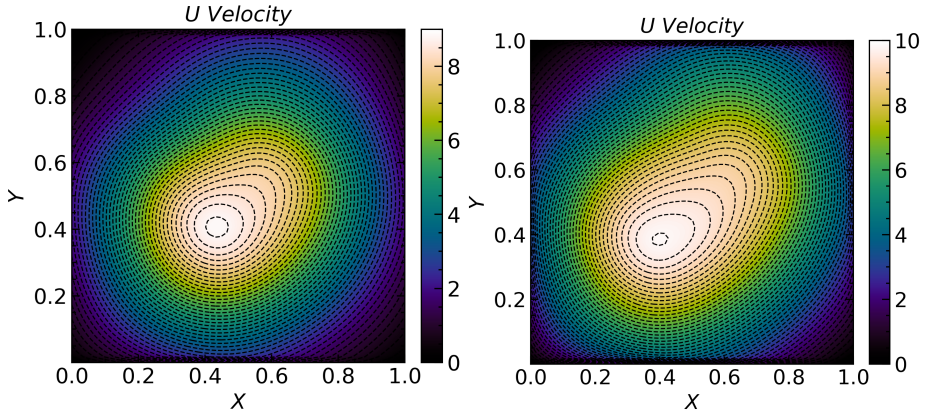


(a)




(b)

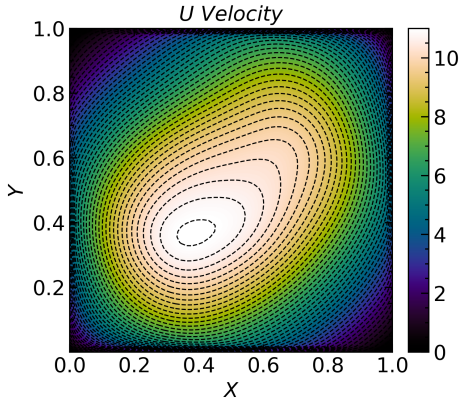


(c)

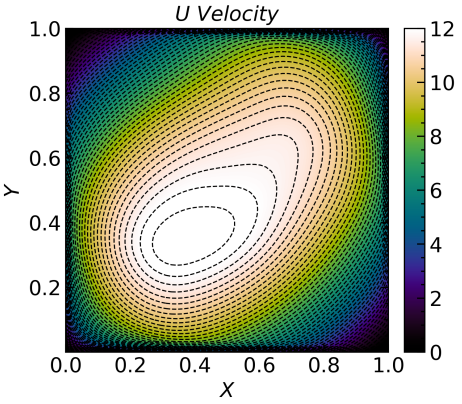


(d)

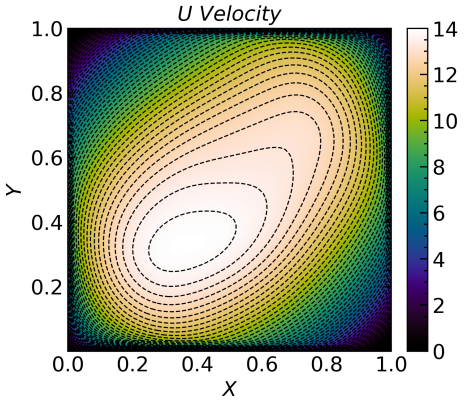


(e)

Figure 4-1: $u$ velocity (in cm/s) for the deterministic test case at a) t = 6 hours, b) t = 12 hours, c) t = 18 hours, d) t = 24 hours, e) t = 30 hours

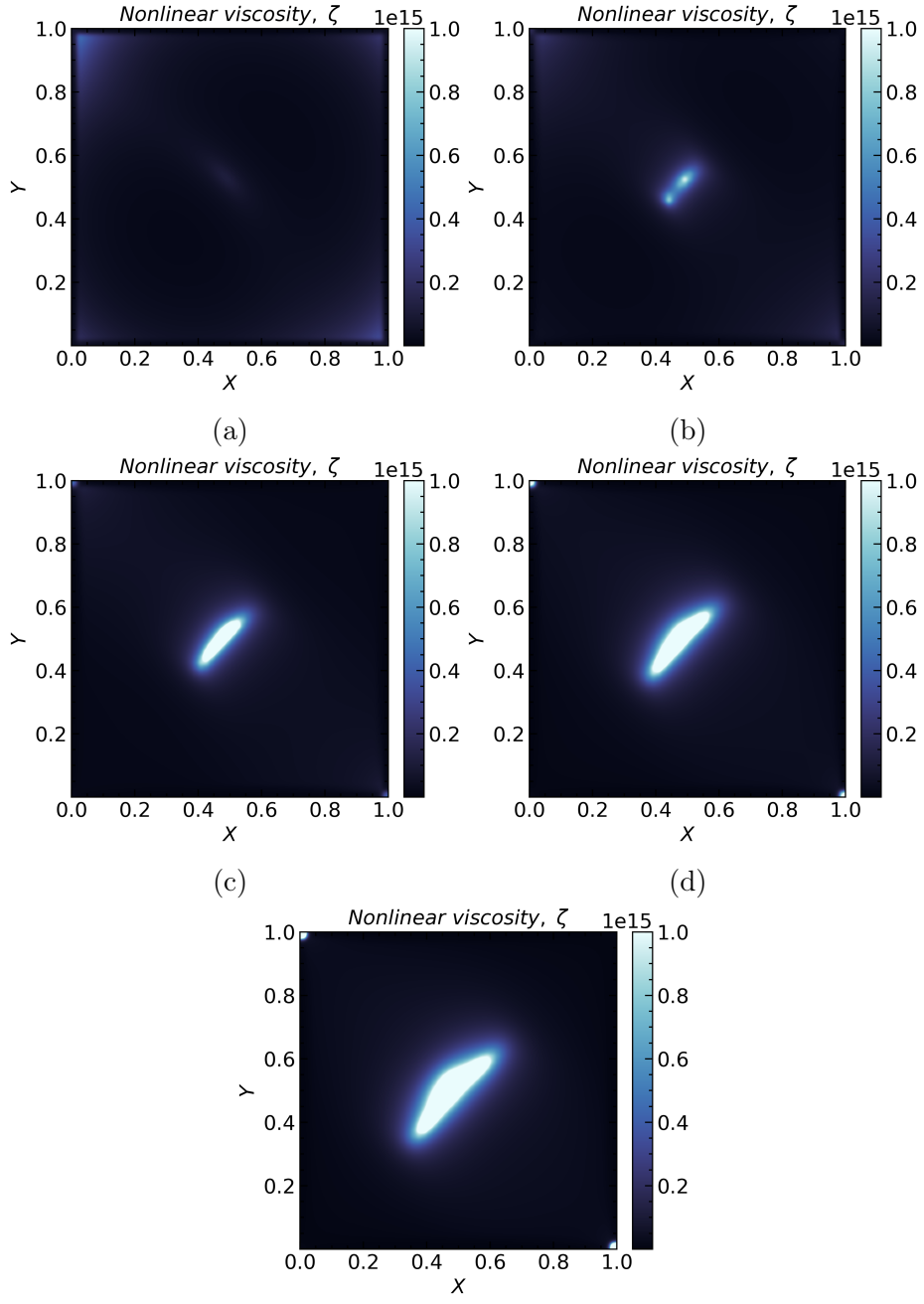


Figure 4-2: Nonlinear viscosity $\zeta$ (in Poise) for the deterministic test case at a) t = 6 hours, b) t = 12 hours, c) t = 18 hours, d) t = 24 hours, e) t = 30 hours

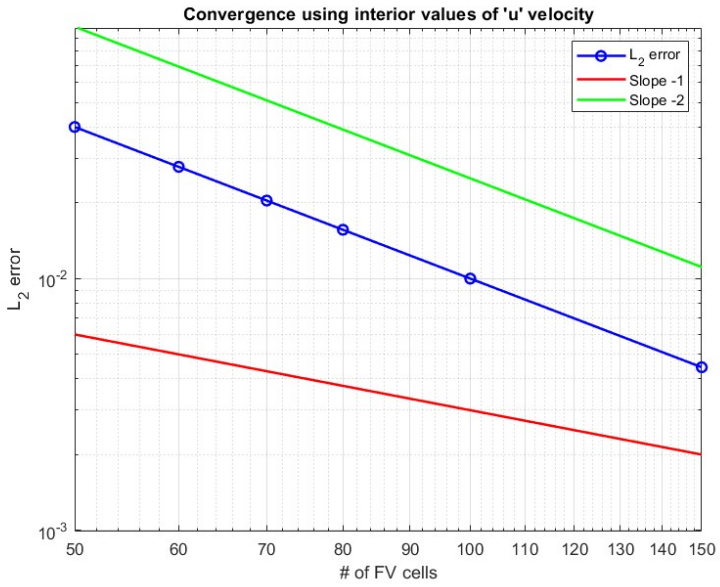


Figure 4-3: Spatial convergence analysis for the deterministic 2D finite volume sea ice solver. We observe second-order convergence which is in agreement with the spatial discretization used (second-order central difference).

initial velocity realizations. The test case and parameters used are a stochastic version

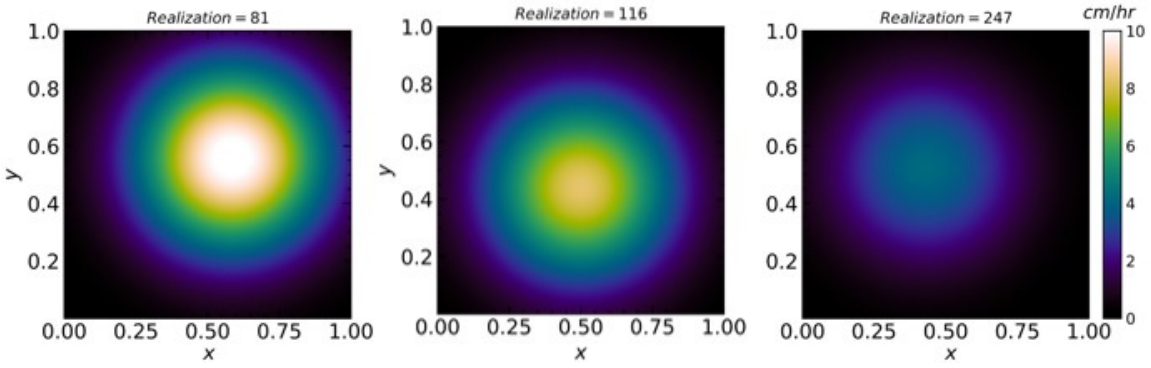


Figure 4-4: Three realizations of the initial stochastic $u$-velocity field

of the test case used in [106] and [43], where a rectangular sheet of ice is surrounded by an ocean and forced by atmospheric wind forcing. The DO-Sea Ice equations are initialized using $n_r = 1000$ realizations as described in Chapter 3.3.1 and evolved numerically using the schemes described in Chapter 3.3.4.

*Test Case 1: Large Ice Sheet Surrounded by Ocean.* The first stochastic test case is that of a large ice sheet surrounded by the ocean. A cyclonic atmospheric forcing

acts on the domain as shown in 4-5. The total size of the domain is 600 km × 600 km. A spatial grid resolution of 5 km × 5 km is used. The concentration of the ice sheet is set to be 0.9. Other parameters used are summarized in table 4.1. An implicit time step of $\Delta t$=30 minutes is used. We select $n_{s,\psi} = 45$, which is a considerable reduction in size compared to $n_r$. This choice of $n_{s,\psi}$ effectively captures 99% of the variance of the system.

Figs. 4-6, 4-7, 4-8, 4-9 and 4-10 show the mean, first two modes and first two stochastic coefficients. We can see that our methodology is able to capture the nonlinear dynamics of sea ice and also capture non-Gaussian distributions of the coefficients at all times.

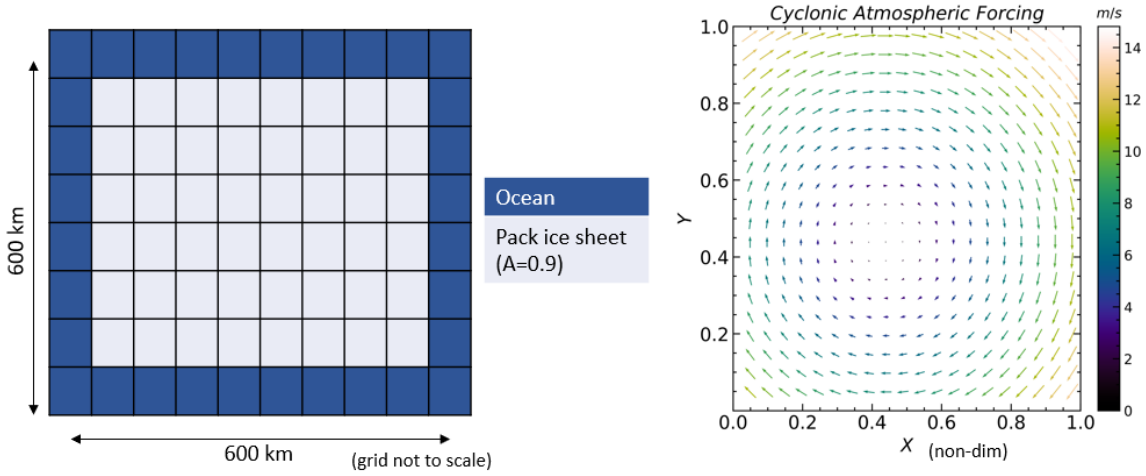


Figure 4-5: Domain and forcing for test case 1 with large ice sheet surrounded by ocean

*Test Case 2: Disconnected Ice Sheets Surrounded by Ocean.* We now use a test case that consists of different types of sea ice. The second stochastic test case is that of disconnected ice sheets surrounded by frozen ice cover and the ocean. A cyclonic atmospheric forcing acts on the domain as shown in 4-11. The total size of the domain is 600 km × 600 km. The disconnected ice blocks each cover 150 km × 150 km and occupy the northeast and southwest corners of the domain. A spatial grid resolution of 5 km × 5 km is used. The concentration of the ice sheet is set to be 0.9, and that of frozen ice cover is set to be 0.65. Other parameters used are summarized in table 4.1. An implicit time step of $\Delta t$=30 minutes is used. We again select $n_{s,\psi} = 45$, which is a

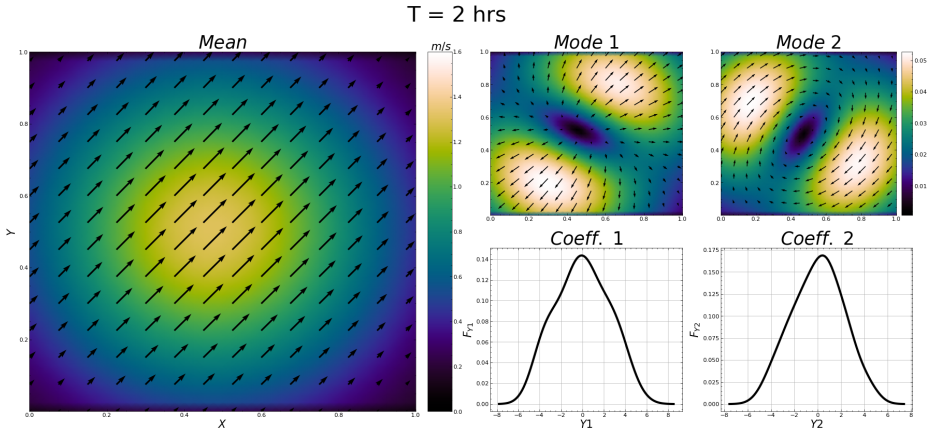


Figure 4-6: DO mean, first two modes and first two stochastic coefficients for test case with a large ice sheet surrounded by the ocean at t=2 hours.

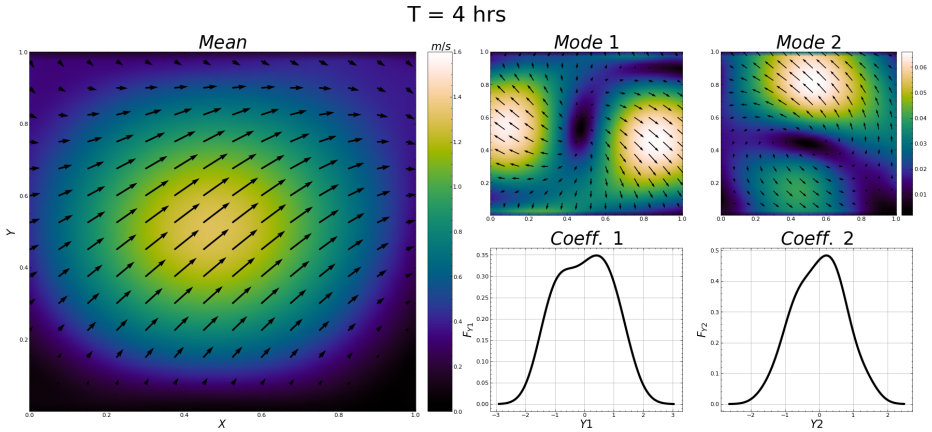


Figure 4-7: DO mean, first two modes and first two stochastic coefficients for test case with a large ice sheet surrounded by the ocean at t=4 hours.

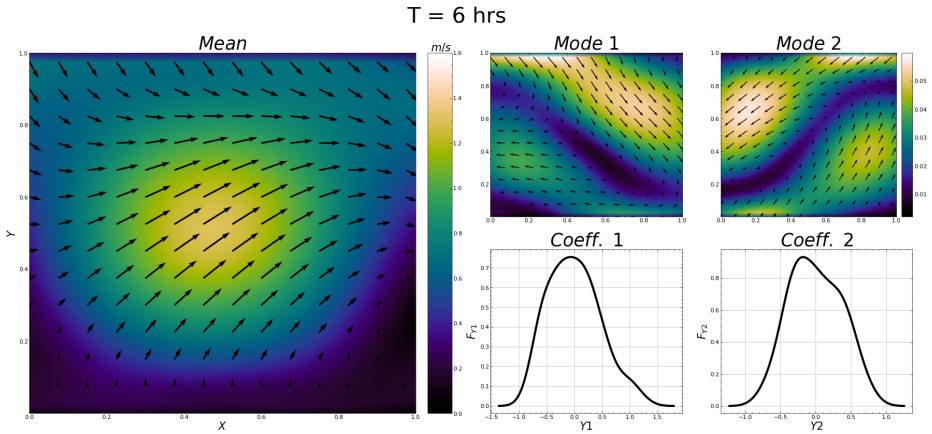


Figure 4-8: DO mean, first two modes and first two stochastic coefficients for test case with a large ice sheet surrounded by the ocean at t=6 hours.

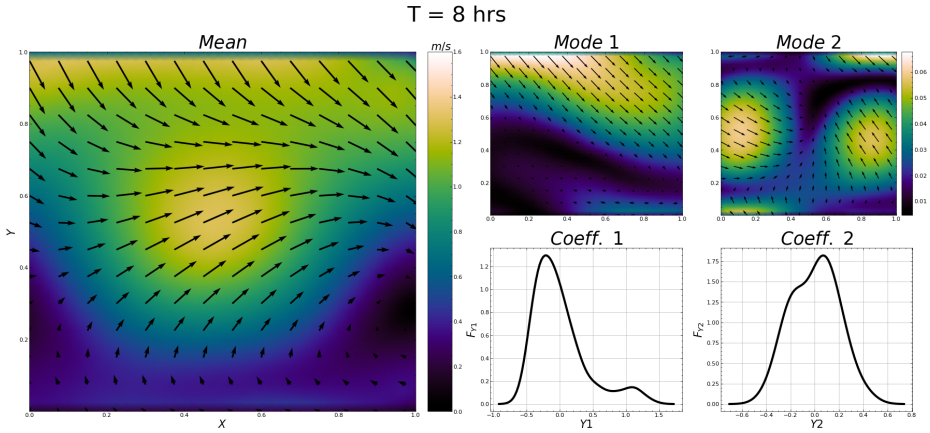


Figure 4-9: DO mean, first two modes and first two stochastic coefficients for test case with a large ice sheet surrounded by the ocean at t=8 hours.

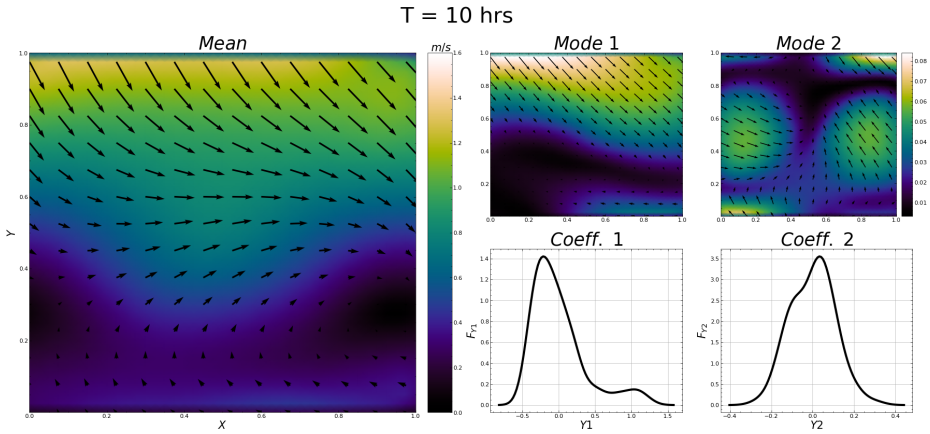


Figure 4-10: DO mean, first two modes and first two stochastic coefficients for test case with a large ice sheet surrounded by the ocean at t=10 hours.

considerable reduction in size compared to $n_r$. This choice of $n_{s,\psi}$ effectively captures 99% of the variance of the system.

Figs. 4-12, 4-13, 4-14, 4-15 and 4-16 show the mean, first two modes and first two stochastic coefficients. We can see that our methodology is able to capture the complex nonlinear dynamics with different sea ice concentrations. We are also able to capture the highly non-Gaussian distributions of the coefficients at all times.

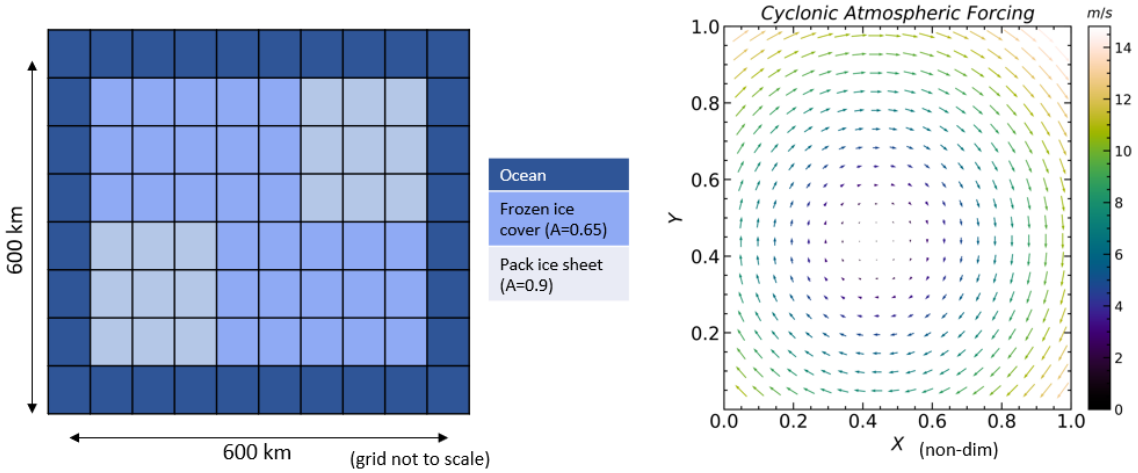


Figure 4-11: Domain and forcing for test case 2 with disconnected ice sheets surrounded by ocean.

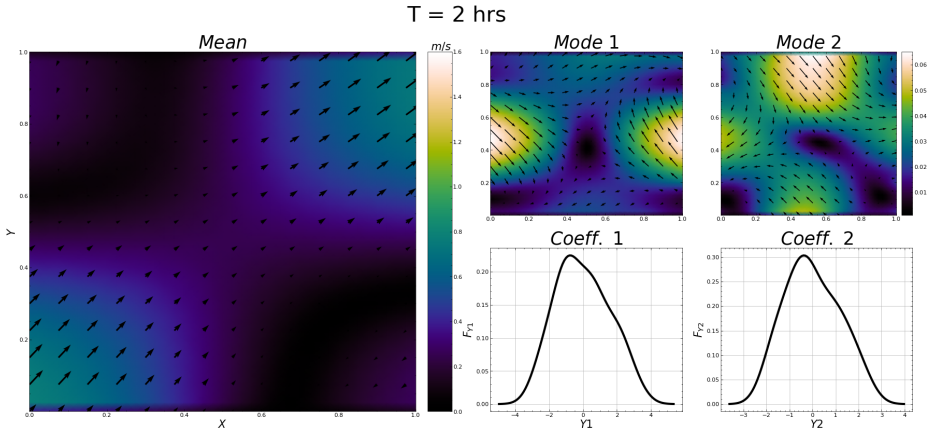


Figure 4-12: DO mean, first two modes and first two stochastic coefficients for test case with disconnected ice sheets surrounded by ocean at t=2 hours.

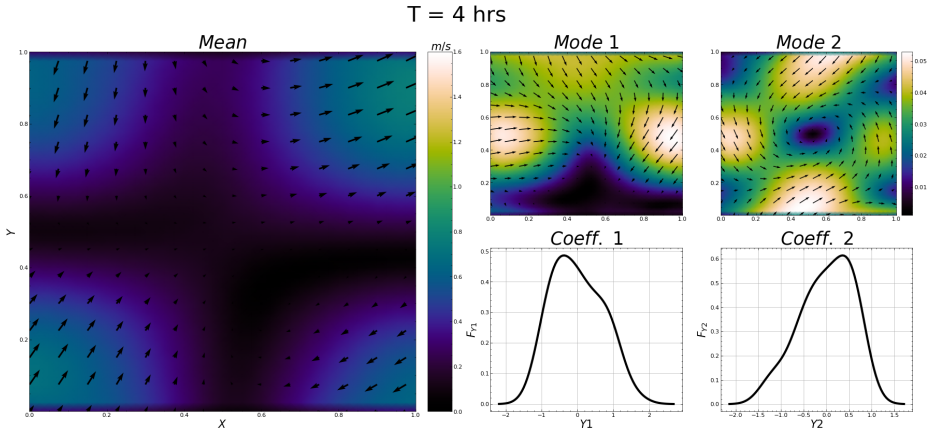


Figure 4-13: DO mean, first two modes and first two stochastic coefficients test case with disconnected ice sheets surrounded by ocean at t=4 hours.

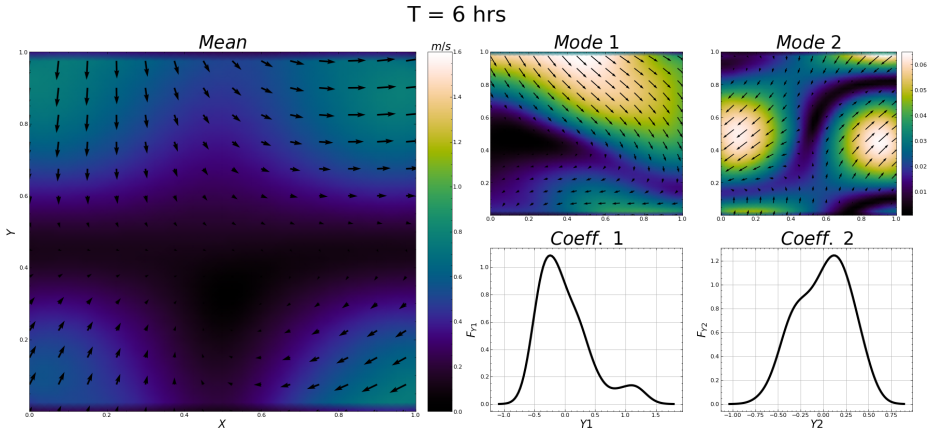


Figure 4-14: DO mean, first two modes and first two stochastic coefficients for test case with disconnected ice sheets surrounded by ocean at t=6 hours.

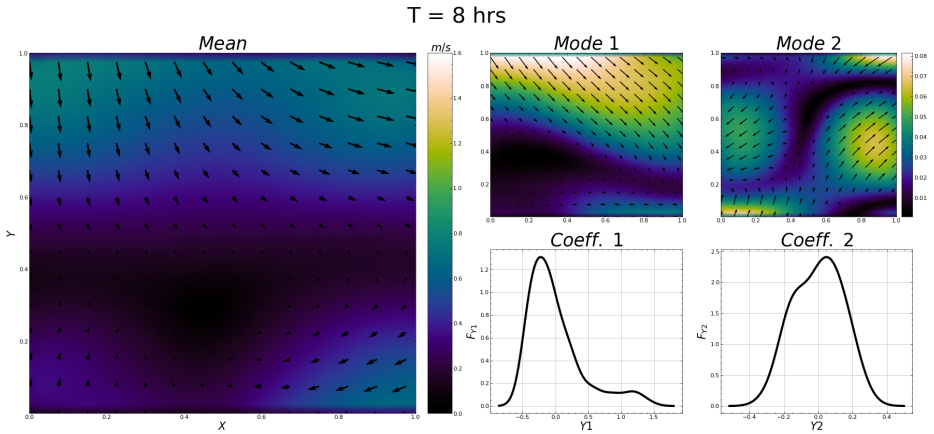


Figure 4-15: DO mean, first two modes and first two stochastic coefficients for test case with disconnected ice sheets surrounded by ocean at t=8 hours.

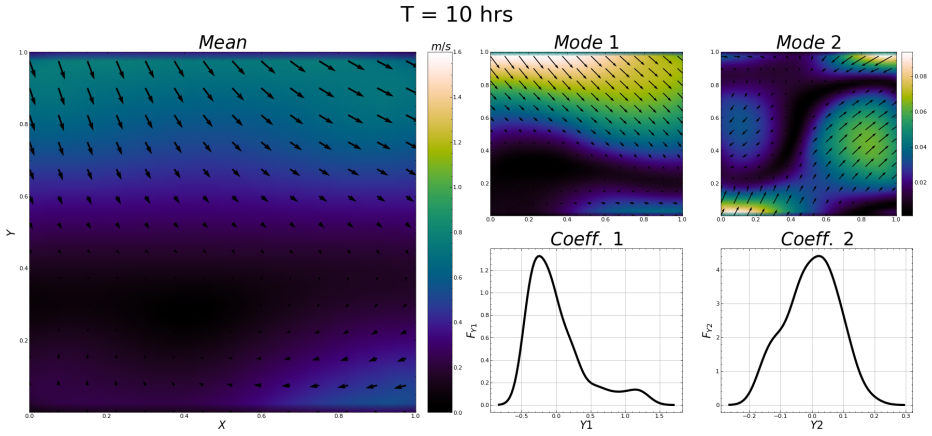


Figure 4-16: DO mean, first two modes and first two stochastic coefficients for test case with disconnected ice sheets surrounded by ocean at t=10 hours.

## 4.3 Discussion

We have showcased that the developed methodology has the ability to evolve uncertainties and capture nonlinear spatiotemporal dynamics and non-Gaussian statistics efficiently. Next, we study the stochastic convergence of the Dynamically Orthogonal-Sea Ice equations as $n_{s,\psi}$ and $n_r$ are increased.

*Convergence with stochastic subspace size.* To study the convergence with stochastic subspace size, we use $n_r = 1000$ coefficient samples and compute the mean field for increasing $n_{s,\psi}$. We then compare the mean field with a true mean field obtained using a direct Monte Carlo method with $n_r = 1000$ members. Figs. 4-17 and 4-18 show that the RMSE of the mean field from the Dynamically Orthogonal-Sea Ice equations decreases significantly as $n_{s,\psi}$ increases for both the test cases. This indicates that the mean field from the Dynamically Orthogonal-Sea Ice equations is indistinguishable from those obtained using Monte Carlo simulations.

*Convergence with number of coefficient samples.* The convergence with number of coefficient samples is also examined. Figs. 4-19 and 4-20 show that the RMSE of the mean field from the Dynamically Orthogonal-Sea Ice equations decreases significantly as $n_r$ increases for both the test cases.

Next, we analyze the computational costs of the Dynamically Orthogonal-Sea Ice equations compared to the direct Monte Carlo method.

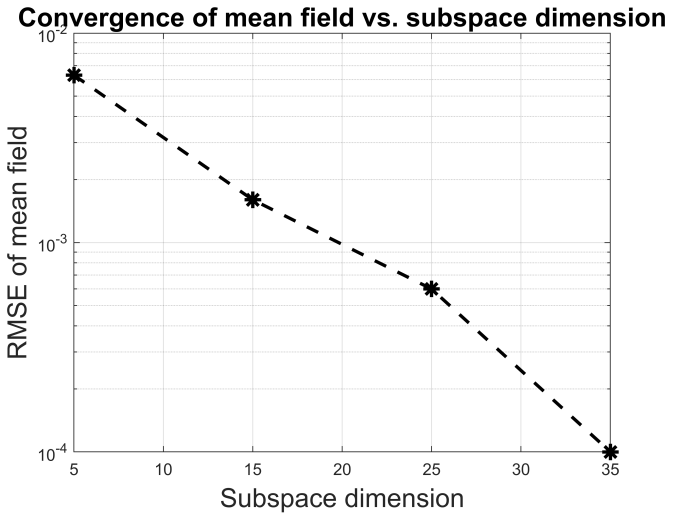


Figure 4-17: Stochastic convergence analysis for the mean velocity field for stochastic test case 1 with increasing stochastic subspace dimension.

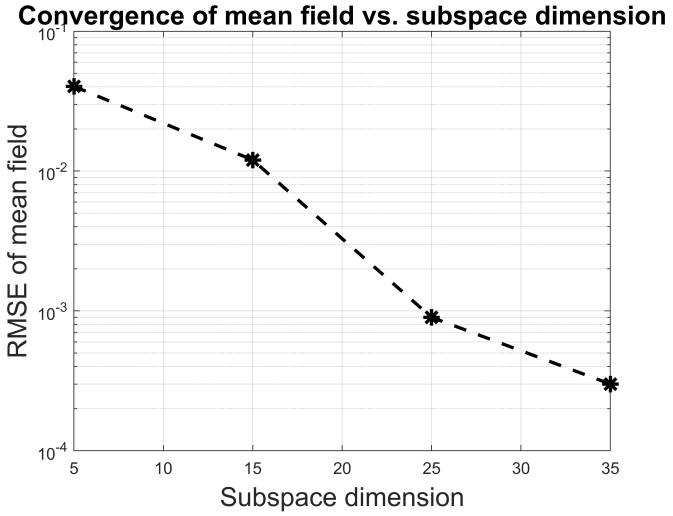


Figure 4-18: Stochastic convergence analysis for the mean velocity field for stochastic test case 2 with increasing stochastic subspace dimension.

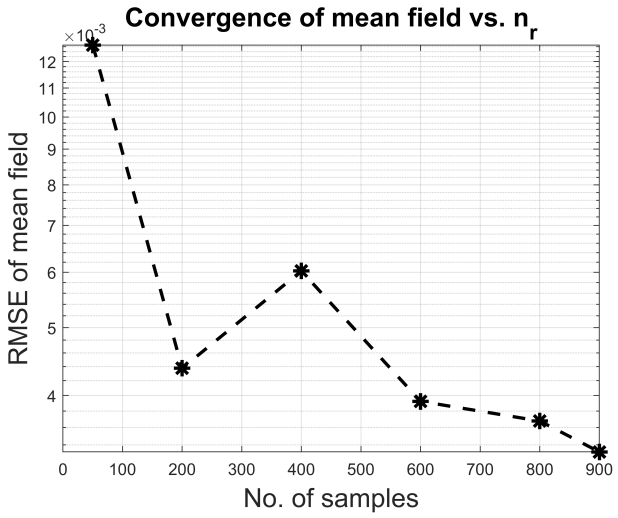


Figure 4-19: Stochastic convergence analysis for the mean velocity field for stochastic test case 1 with increasing number of coefficient samples.

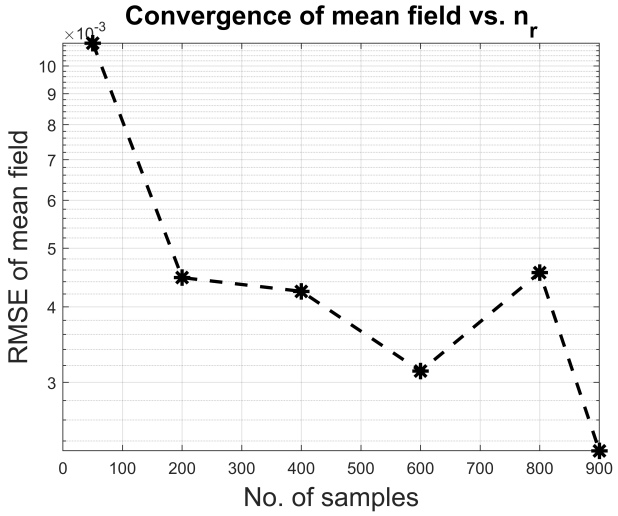


Figure 4-20: Stochastic convergence analysis for the mean velocity field for stochastic test case 2 with increasing number of coefficient samples.

*Computational and memory costs.* The cost of solving the deterministic sea ice equations is dominated by the linear solve for the momentum equations. For a system of $n_{d,\psi}$ discrete state variables, this requires solving a linear system of size $n_{d,\psi} \times n_{d,\psi}$. Solving this system typically has a cost of $\mathcal{O}(n_{d,\psi}^{\lambda})$ where $1 \leq \lambda < 2$ depends on the numerical scheme and algorithm used. Hence, using a direct Monte Carlo method for $n_r$ realizations has a total cost of $\mathcal{O}(n_r n_{d,\psi}^{\lambda})$. The cost of solving the DO mean equation is similar to that of the deterministic equations and has cost $\mathcal{O}(n_{d,\psi}^{\lambda})$. The cost of solving the DO mode equations is $\mathcal{O}(n_{s,\psi} n_{d,\psi}^{\lambda})$ for the linear system solve. For typical sea ice applications where $n_{d,\psi} \gg n_{s,\psi}$, the cost of the linear system solve dominates the cost of projections in the DO mode equations. The cost of solving the DO coefficient equations is also negligible since they are just stochastic ODEs while the DO mean and DO mode equations are PDEs. Hence, we get the ratio of costs of the DO Sea Ice equations to the MC method as

$$\frac{\text{Cost}_{DO}}{\text{Cost}_{MC}} \to \frac{(n_{s,\psi}+1) n_{d,\psi}^{\lambda}}{n_r n_{d,\psi}^{\lambda}} \tag{4.2}$$

$$\frac{\text{Cost}_{DO}}{\text{Cost}_{MC}} \sim \frac{(n_{s,\psi}+1)}{n_r} \tag{4.3}$$

This showcases the significant increase in computational efficiency achieved by using the DO Sea Ice equations since $n_r \gg n_{s,\psi}$ for typical sea ice applications.

In terms of memory costs, the direct Monte Carlo method has memory costs of $\mathcal{O}(n_r n_{d,\psi})$. The DO mean has memory costs of $\mathcal{O}(n_{d,\psi})$, while the modes have costs of $\mathcal{O}(n_{s,\psi} n_{d,\psi})$ and coefficients have cost of $\mathcal{O}(n_r n_{s,\psi})$. Hence, we get the ratio of memory costs of the DO Sea Ice equations to the MC method as

$$\frac{\text{Memory}_{DO}}{\text{Memory}_{MC}} \to \frac{(n_{s,\psi}+1) n_{d,\psi} + n_r n_{s,\psi}}{n_r n_{d,\psi}} \tag{4.4}$$

This again showcases the significant increase in memory efficiency achieved by using the DO Sea Ice equations since $n_r \gg n_{s,\psi}$ and $n_{d,\psi} \gg n_{s,\psi}$ for typical sea ice applications.

# Chapter 5

# Conclusions and Future Work

In this work, we developed new stochastic sea ice models and schemes using the Dynamically Orthogonal (DO) equations for probabilistic modeling. First, we implemented and verified a deterministic 2D viscoplastic sea ice solver. We observed second-order convergence to spatial discretization as expected. Next, we derived and implemented the new stochastic Dynamically Orthogonal-Sea Ice equations and numerical schemes. We illustrated and evaluated the ability of our new stochastic sea ice modeling and schemes to evolve uncertainties and capture nonlinear spatiotemporal dynamics and non-Gaussian statistics efficiently using two idealized test cases, 1) large ice sheet surrounded by the ocean, 2) disconnected ice blocks surrounded by the ocean. We studied the convergence to the stochastic subspace size, and number of coefficient samples. We showcased the computational efficiency of the new stochastic Dynamically Orthogonal-Sea Ice equations over the direct Monte Carlo method.

Since, the developed equations and schemes perform well for the sea ice momentum equations, we are currently working on extending the method to capture sea ice height and concentration uncertainties. We plan to evaluate our methodology using more realistic stochastic sea ice test cases. We are also investigating numerical methods with fully implicit time integration, such as schemes using the Jacobian-Free Newton-Krylov method, which could provide additional computational and memory efficiency [57, 58].

The DO Sea Ice equations can be combined with the Gaussian Mixture Model

(GMM-DO) filter [108, 109] for Bayesian data assimilation of sparse, noisy data and learning parameters, states and even model formulations themselves from data [31, 82]. Another research opportunity is to use neural closure models [32, 30, 47] to capture missing sea ice features such as leads and ridges and other subgrid-scale distributions [118].

The inclusion of sea ice dynamics would enhance the capabilities of the Multidisciplinary Simulation, Estimation, and Assimilation Systems (MSEAS) [87, 35, 34, 33] software, allowing for sea-ice-ocean-atmospheric coupling, and usage of realistic ocean currents and atmospheric forcing. The software has been used for fundamental research and realistic simulations in various parts of the world [73, 33, 68, 111, 53, 29, 70, 2]. Such coupled models would also help capitalize on other capabilities of the MSEAS software including ensemble forecasting and data assimilation [64, 61, 60, 63, 71], reduced-order modeling [19, 11, 36, 100, 99], and path planning and adaptive sampling [67, 68, 66, 63, 17].

# Bibliography


[1] Alen Alexanderian. A brief note on the karhunen-lo\eve expansion. *arXiv preprint arXiv:1509.07526*, 2015.

[2] Wael Hajj Ali, Aaron Charous, Chris Mirabito, Patrick J. Haley, Jr., and Pierre F. J. Lermusiaux. MSEAS-ParEq for ocean-acoustic modeling around the globe. In *OCEANS 2023 IEEE/MTS Gulf Coast*, Biloxi, MS, September 2023. IEEE. In press.

[3] Terje Aven. *Quantitative risk assessment: the scientific platform*. Cambridge university press, 2011.

[4] Nicholas Beaudoin and Barry Naughton. Chinese arctic exploitation. 2014.

[5] Berill Blair, Malte Müller, Cyril Palerme, Rayne Blair, David Crookall, Maaike Knol-Kauffman, and Machiel Lamers. Coproducing sea ice predictions with stakeholders using simulation. *Weather, Climate, and Society*, 14(2):399–413, 2022.

[6] E Blanchard-Wrigglesworth, RI Cullather, W Wang, J Zhang, and CM Bitz. Model forecast skill and sensitivity to initial conditions in the seasonal sea ice outlook. *Geophysical Research Letters*, 42(19):8042–8048, 2015.

[7] Scott G Borgerson. Arctic meltdown-the economic and security implications of global warming. *Foreign Aff.*, 87:63, 2008.

[8] Sylvain Bouillon, Miguel Angel Morales Maqueda, Vincent Legat, and Thierry Fichefet. An elastic–viscous–plastic sea ice model formulated on arakawa b and c grids. *Ocean Modelling*, 27(3-4):174–184, 2009.

[9] Kevin Bulthuis, Maarten Arnst, Sainan Sun, and Frank Pattyn. Uncertainty quantification of the multi-centennial response of the antarctic ice sheet to climate change. *The Cryosphere*, 13(4):1349–1380, 2019.

[10] Aaron Charous. *Dynamical Reduced-Order Models for High-Dimensional Systems*. PhD thesis, Massachusetts Institute of Technology, Department of Mechanical Engineering and Center for Computational Science and Engineering, Cambridge, Massachusetts, June 2023.

[11] Aaron Charous and Pierre F. J. Lermusiaux. Dynamically orthogonal differential equations for stochastic and deterministic reduced-order modeling of ocean acoustic wave propagation. In *OCEANS 2021 IEEE/MTS*, pages 1–7. IEEE, September 2021.

[12] Aaron Charous and Pierre F. J. Lermusiaux. Dynamically orthogonal Runge–Kutta schemes with perturbative retractions for the dynamical low-rank approximation. *SIAM Journal on Scientific Computing*, 45(2):A872–A897, 2023.

[13] Aaron Charous and Pierre F. J. Lermusiaux. Stable rank-adaptive dynamically orthogonal Runge–Kutta schemes. *SIAM Journal on Scientific Computing*, 2023. In press.

[14] Sukun Cheng, Ali Aydoğdu, Pierre Rampal, Alberto Carrassi, and Laurent Bertino. Probabilistic forecasts of sea ice trajectories in the arctic: impact of uncertainties in surface wind and ice cohesion. In *Oceans*, volume 1, pages 326–342. MDPI, 2020.

[15] MD Coon, GA Maykut, and RS Pritchard. Modeling the pack ice as an elastic-plastic material. 1974.

[16] A Dirkson, B Denis, and WJ Merryfield. A multimodel approach for improving seasonal probabilistic forecasts of regional arctic sea ice. *Geophysical Research Letters*, 46(19):10844–10853, 2019.

[17] Manan M. Doshi, Manmeet S. Bhabra, and Pierre F. J. Lermusiaux. Energy-time optimal path planning in dynamic flows: Theory and schemes. *Computer Methods in Applied Mechanics and Engineering*, 405:115865, February 2023.

[18] Daniel L Feltham. Sea ice rheology. *Annu. Rev. Fluid Mech.*, 40:91–112, 2008.

[19] Florian Feppon and Pierre F. J. Lermusiaux. Dynamically orthogonal numerical schemes for efficient stochastic advection and Lagrangian transport. *SIAM Review*, 60(3):595–625, 2018.

[20] Florian Feppon and Pierre F. J. Lermusiaux. A geometric approach to dynamical model-order reduction. *SIAM Journal on Matrix Analysis and Applications*, 39(1):510–538, 2018.

[21] Florian Feppon and Pierre F. J. Lermusiaux. The extrinsic geometry of dynamical systems tracking nonlinear matrix projections. *SIAM Journal on Matrix Analysis and Applications*, 40(2):814–844, 2019.

[22] GM Flato and WD Hibler. On a simple sea-ice dynamics model for climate studies. *Annals of Glaciology*, 14:72–77, 1990.

[23] Roger Ghanem and Pol D Spanos. Polynomial chaos in stochastic finite elements. 1990.

[24] Kenneth M Golden, Luke G Bennetts, Elena Cherkaev, Ian Eisenman, Daniel Feltham, Christopher Horvat, Elizabeth Hunke, Christopher Jones, Donald K Perovich, Pedro Ponte-Castaneda, et al. Modeling sea ice. 2020.

[25] Mats Granskog, Hermanni Kaartokallio, Harri Kuosa, David N Thomas, and Jouni Vainio. Sea ice in the baltic sea–a review. *Estuarine, Coastal and Shelf Science*, 70(1-2):145–160, 2006.

[26] Colin Grudzien and Marc Bocquet. A tutorial on bayesian data assimilation. *arXiv preprint arXiv:2112.07704*, 2021.

[27] Abhinav Gupta. *Scientific Machine Learning for Dynamical Systems: Theory and Applications to Fluid Flow and Ocean Ecosystem Modeling*. PhD thesis, Massachusetts Institute of Technology, Department of Mechanical Engineering, Cambridge, Massachusetts, September 2022.

[28] Abhinav Gupta, Wael Hajj Ali, and Pierre F. J. Lermusiaux. Boundary conditions for stochastic DO equations. MSEAS Report, Department of Mechanical Engineering, Massachusetts Institute of Technology, Cambridge, MA, 2016.

[29] Abhinav Gupta, Patrick J. Haley, Deepak N. Subramani, and Pierre F. J. Lermusiaux. Fish modeling and Bayesian learning for the Lakshadweep Islands. In *OCEANS 2019 MTS/IEEE SEATTLE*, pages 1–10, Seattle, October 2019. IEEE.

[30] Abhinav Gupta and Pierre F. J. Lermusiaux. Neural closure models for dynamical systems. *Proceedings of The Royal Society A*, 477(2252):1–29, August 2021.

[31] Abhinav Gupta and Pierre F. J. Lermusiaux. Bayesian learning of coupled biogeochemical-physical models. *Progress in Oceanography*, 216:103050, May 2023.

[32] Abhinav Gupta and Pierre F. J. Lermusiaux. Generalized neural closure models with interpretability. *Scientific Reports*, 2023. In press.

[33] P. J. Haley, Jr., P. F. J. Lermusiaux, A. R. Robinson, W. G. Leslie, O. Logoutov, G. Cossarini, X. S. Liang, P. Moreno, S. R. Ramp, J. D. Doyle, J. Bellingham, F. Chavez, and S. Johnston. Forecasting and reanalysis in the Monterey Bay/California Current region for the Autonomous Ocean Sampling Network-II experiment. *Deep Sea Research Part II: Topical Studies in Oceanography*, 56(3–5):127–148, February 2009.

[34] Patrick J. Haley, Jr., Arpit Agarwal, and Pierre F. J. Lermusiaux. Optimizing velocities and transports for complex coastal regions and archipelagos. *Ocean Modelling*, 89:1–28, May 2015.

[35] Patrick J. Haley, Jr. and Pierre F. J. Lermusiaux. Multiscale two-way embedding schemes for free-surface primitive equations in the "Multidisciplinary Simulation, Estimation and Assimilation System". *Ocean Dynamics*, 60(6):1497–1537, December 2010.

[36] Jacob P. Heuss, Patrick J. Haley, Jr., Chris Mirabito, Emanuel Coelho, Martha C. Schönau, Kevin Heaney, and Pierre F. J. Lermusiaux. Reduced order modeling for stochastic prediction onboard autonomous platforms at sea. In *OCEANS 2020 IEEE/MTS*, pages 1–10. IEEE, October 2020.

[37] W DIII Hibler. A dynamic thermodynamic sea ice model. *Journal of physical oceanography*, 9(4):815–846, 1979.

[38] WD Hibler III. A viscous sea ice law as a stochastic average of plasticity. *Journal of Geophysical Research*, 82(27):3932–3938, 1977.

[39] Joshua Ho. The implications of arctic sea ice decline on shipping. *Marine Policy*, 34(3):713–715, 2010.

[40] Malte Humpert and Andreas Raspotnik. The future of arctic shipping. *Port Technology International*, 55(11):10–11, 2012.

[41] Elizabeth Hunke, Richard Allard, Philippe Blain, Ed Blockley, Daniel Feltham, Thierry Fichefet, Gilles Garric, Robert Grumbine, Jean-François Lemieux, Till Rasmussen, et al. Should sea-ice modeling tools designed for climate research be used for short-term forecasting? *Current Climate Change Reports*, 6:121–136, 2020.

[42] Elizabeth C Hunke. Viscous–plastic sea ice dynamics with the evp model: Linearization issues. *Journal of Computational Physics*, 170(1):18–38, 2001.

[43] Elizabeth C Hunke and John K Dukowicz. An elastic–viscous–plastic model for sea ice dynamics. *Journal of Physical Oceanography*, 27(9):1849–1867, 1997.

[44] Elizabeth C Hunke, William H Lipscomb, and Adrian K Turner. Sea-ice models for climate study: retrospective and new directions. *Journal of Glaciology*, 56(200):1162–1172, 2010.

[45] Elizabeth C Hunke, William H Lipscomb, Adrian K Turner, Nicole Jeffery, and Scott Elliott. Cice: the los alamos sea ice model documentation and software userâs manual version 4.1 la-cc-06-012. *T-3 Fluid Dynamics Group, Los Alamos National Laboratory*, 675:500, 2010.

[46] Chi F Ip, William D Hibler, and Gregory M Flato. On the effect of rheology on seasonal sea-ice simulations. *Annals of Glaciology*, 15:17–25, 1991.

[47] Aman Jalan. Neural closure models for chaotic dynamical systems. Master's thesis, Massachusetts Institute of Technology, Cambridge, Massachusetts, February 2023.

[48] Stephan Juricke and Thomas Jung. Influence of stochastic sea ice parametrization on climate and the role of atmosphere–sea ice–ocean interaction. *Philosophical Transactions of the Royal Society A: Mathematical, Physical and Engineering Sciences*, 372(2018):20130283, 2014.

[49] Vladimir M Kattsov, Vladimir E Ryabinin, James E Overland, Mark C Serreze, Martin Visbeck, John E Walsh, Walt Meier, and Xiangdong Zhang. Arctic sea-ice change: a grand challenge of climate science. *Journal of Glaciology*, 56(200):1115–1121, 2010.

[50] Othmar Koch and Christian Lubich. Dynamical low-rank approximation. *SIAM Journal on Matrix Analysis and Applications*, 29(2):434–454, 2007.

[51] Martin Kreyscher, Markus Harder, Peter Lemke, and Gregory M Flato. Results of the sea ice model intercomparison project: Evaluation of sea ice rheology schemes for use in climate simulations. *Journal of Geophysical Research: Oceans*, 105(C5):11299–11320, 2000.

[52] Michael Kuhn. The nutrient cycle through snow and ice, a review. *Aquatic Sciences*, 63:150–167, 2001.

[53] C. S. Kulkarni, P. J. Haley, Jr., P. F. J. Lermusiaux, A. Dutt, A. Gupta, C. Mirabito, D. N. Subramani, S. Jana, W. H. Ali, T. Peacock, C. M. Royo, A. Rzeznik, and R. Supekar. Real-time sediment plume modeling in the Southern California Bight. In *OCEANS Conference 2018*, Charleston, SC, October 2018. IEEE.

[54] Laura L Landrum and Marika M Holland. Influences of changing sea ice and snow thicknesses on simulated arctic winter heat fluxes. *The Cryosphere*, 16(4):1483–1495, 2022.

[55] Olivier Le Maître and Omar M Knio. *Spectral methods for uncertainty quantification: with applications to computational fluid dynamics*. Springer Science & Business Media, 2010.

[56] Jean-François Lemieux, Dana A Knoll, Bruno Tremblay, David M Holland, and Martin Losch. A comparison of the jacobian-free newton–krylov method and the evp model for solving the sea ice momentum equation with a viscous-plastic formulation: A serial algorithm study. *Journal of Computational Physics*, 231(17):5926–5944, 2012.

[57] Jean-François Lemieux and Bruno Tremblay. Numerical convergence of viscous-plastic sea ice models. *Journal of Geophysical Research: Oceans*, 114(C5), 2009.

[58] Jean-François Lemieux, Bruno Tremblay, Jan Sedláček, Paul Tupper, Stephen Thomas, David Huard, and Jean-Pierre Auclair. Improving the numerical convergence of viscous-plastic sea ice models with the jacobian-free newton–krylov method. *Journal of Computational Physics*, 229(8):2840–2852, 2010.

[59] Matti Leppäranta. *The drift of sea ice*. Springer Science & Business Media, 2011.

[60] P. F. J. Lermusiaux. Estimation and study of mesoscale variability in the Strait of Sicily. *Dynamics of Atmospheres and Oceans*, 29(2):255–303, 1999.

[61] P. F. J. Lermusiaux. On the mapping of multivariate geophysical fields: Sensitivities to size, scales, and dynamics. *Journal of Atmospheric and Oceanic Technology*, 19(10):1602–1637, 2002.

[62] P. F. J. Lermusiaux. Uncertainty estimation and prediction for interdisciplinary ocean dynamics. *Journal of Computational Physics*, 217(1):176–199, 2006.

[63] P. F. J Lermusiaux. Adaptive modeling, adaptive data assimilation and adaptive sampling. *Physica D: Nonlinear Phenomena*, 230(1):172–196, 2007.

[64] P. F. J. Lermusiaux, D. G. M. Anderson, and C. J. Lozano. On the mapping of multivariate geophysical fields: Error and variability subspace estimates. *Quarterly Journal of the Royal Meteorological Society*, 126(565):1387–1429, 2000.

[65] P. F. J. Lermusiaux, C.-S. Chiu, G. G. Gawarkiewicz, P. Abbot, A. R. Robinson, R. N. Miller, P. J. Haley, Jr, W. G. Leslie, S. J. Majumdar, A. Pang, and F. Lekien. Quantifying uncertainties in ocean predictions. *Oceanography*, 19(1):92–105, 2006.

[66] P. F. J Lermusiaux, P. J. Haley, Jr, and N. K. Yilmaz. Environmental prediction, path planning and adaptive sampling: sensing and modeling for efficient ocean monitoring, management and pollution control. *Sea Technology*, 48(9):35–38, 2007.

[67] P. F. J. Lermusiaux, T. Lolla, P. J. Haley, Jr., K. Yigit, M. P. Ueckermann, T. Sondergaard, and W. G. Leslie. Science of autonomy: Time-optimal path planning and adaptive sampling for swarms of ocean vehicles. In Tom Curtin, editor, *Springer Handbook of Ocean Engineering: Autonomous Ocean Vehicles, Subsystems and Control*, chapter 21, pages 481–498. Springer, 2016.

[68] P. F. J. Lermusiaux, D. N. Subramani, J. Lin, C. S. Kulkarni, A. Gupta, A. Dutt, T. Lolla, P. J. Haley, Jr., W. H. Ali, C. Mirabito, and S. Jana. A future for intelligent autonomous ocean observing systems. *Journal of Marine Research*, 75(6):765–813, November 2017. The Sea. Volume 17, The Science of Ocean Prediction, Part 2.

[69] Pierre F. J. Lermusiaux. Numerical fluid mechanics. MIT OpenCourseWare, May 2015.

[70] Pierre F. J. Lermusiaux, Manan Doshi, Chinmay S. Kulkarni, Abhinav Gupta, Patrick J. Haley, Jr., Chris Mirabito, Francesco Trotta, S. J. Levang, G. R. Flierl, J. Marshall, Thomas Peacock, and C. Noble. Plastic pollution in the

coastal oceans: Characterization and modeling. In *OCEANS 2019 MTS/IEEE SEATTLE*, pages 1–10, Seattle, October 2019. IEEE.

[71] Pierre F. J. Lermusiaux, Chris Mirabito, Patrick J. Haley, Jr., Wael Hajj Ali, Abhinav Gupta, Sudip Jana, Eugene Dorfman, Alison Laferriere, Aaron Kofford, G. Shepard, M. Goldsmith, Kevin Heaney, Emanuel Coelho, J. Boyle, J. Murray, L. Freitag, and A. Morozov. Real-time probabilistic coupled ocean physics-acoustics forecasting and data assimilation for underwater GPS. In *OCEANS 2020 IEEE/MTS*, pages 1–9. IEEE, October 2020.

[72] Pierre F. J. Lermusiaux and A. R. Robinson. Data assimilation via Error Subspace Statistical Estimation, part I: Theory and schemes. *Monthly Weather Review*, 127(7):1385–1407, 1999.

[73] W. G. Leslie, A. R. Robinson, P. J. Haley, Jr, O. Logutov, P. A. Moreno, P. F. J. Lermusiaux, and E. Coelho. Verification and training of real-time forecasting of multi-scale ocean dynamics for maritime rapid environmental assessment. *Journal of Marine Systems*, 69(1):3–16, 2008.

[74] Tongtong Li, Anne Gelb, and Yoonsang Lee. Improving numerical accuracy for the viscous-plastic formulation of sea ice. *Journal of Computational Physics*, 487:112184, 2023.

[75] Jing Lin. *Bayesian Learning for High-Dimensional Nonlinear Systems: Methodologies, Numerics and Applications to Fluid Flows*. PhD thesis, Massachusetts Institute of Technology, Department of Mechanical Engineering, Cambridge, Massachusetts, September 2020.

[76] Jing Lin and Pierre F. J. Lermusiaux. Minimum-correction second-moment matching: Theory, algorithms and applications. *Numerische Mathematik*, 147(3):611–650, March 2021.

[77] Rebecca Lindsey and Michon Scott. Climate change: Arctic sea ice summer minimum. *Website: https://tinyurl. com/3x7knf28*, 2020.

[78] M Loève. Probability theory, vol. ii, volume 46 of. *Graduate Texts in Mathematics*.

[79] Martin Losch and Sergey Danilov. On solving the momentum equations of dynamic sea ice models with implicit solvers and the elastic–viscous–plastic technique. *Ocean Modelling*, 41:42–52, 2012.

[80] Martin Losch, Annika Fuchs, Jean-François Lemieux, and Anna Vanselow. A parallel jacobian-free newton–krylov solver for a coupled sea ice-ocean model. *Journal of Computational Physics*, 257:901–911, 2014.

[81] Martin Losch, Dimitris Menemenlis, Jean-Michel Campin, Patick Heimbach, and Chris Hill. On the formulation of sea-ice models. part 1: Effects of different

solver implementations and parameterizations. *Ocean Modelling*, 33(1-2):129–144, 2010.

[82] Peter Lu and Pierre F. J. Lermusiaux. Bayesian learning of stochastic dynamical models. *Physica D: Nonlinear Phenomena*, 427:133003, December 2021.

[83] Peter Guang Yi Lu. Bayesian inference of stochastic dynamical models. Master's thesis, Massachusetts Institute of Technology, Department of Mechanical Engineering, Cambridge, Massachusetts, February 2013.

[84] François Massonnet, Thierry Fichefet, Hugues Goosse, Martin Vancoppenolle, Pierre Mathiot, and C König Beatty. On the influence of model physics on simulations of arctic and antarctic sea ice. *The Cryosphere*, 5(3):687–699, 2011.

[85] MG McPhee. Ice-ocean momentum transfer for the aidjex ice model. *Aidjex Bull*, 29:93–111, 1975.

[86] C Mehlmann and T Richter. A modified global newton solver for viscous-plastic sea ice models. *Ocean Modelling*, 116:96–107, 2017.

[87] MSEAS Group. MSEAS Software, 2013.

[88] Josef M Oberhuber. Simulation of the atlantic circulation with a coupled sea ice-mixed layer-isopycnal general circulation model. part i: Model description. *Journal of Physical Oceanography*, 23(5):808–829, 1993.

[89] James E Overland and Muyin Wang. When will the summer arctic be nearly sea ice free? *Geophysical Research Letters*, 40(10):2097–2101, 2013.

[90] Kara J Peterson, Pavel Blagoveston Bochev, and Biliana S Paskaleva. Development, sensitivity analysis, and uncertainty quantification of high-fidelity arctic sea ice models. Technical report, Sandia National Laboratories (SNL), Albuquerque, NM, and Livermore, CA âŠ, 2010.

[91] Nicholas W Pilfold, Alysa McCall, Andrew E Derocher, Nicholas J Lunn, and Evan Richardson. Migratory response of polar bears to sea ice loss: to swim or not to swim. *Ecography*, 40(1):189–199, 2017.

[92] Siva Prasad, Ronald D Haynes, Igor Zakharov, and Thomas Puestow. Estimation of sea ice parameters using an assimilated sea ice model with a variable drag formulation. *Ocean Modelling*, 158:101739, 2021.

[93] Matthias Rabatel, Pierre Rampal, Alberto Carrassi, Laurent Bertino, and Christopher KRT Jones. Impact of rheology on probabilistic forecasts of sea ice trajectories: application for search and rescue operations in the arctic. *The Cryosphere*, 12(3):935–953, 2018.

[94] JGL Rae, HT Hewitt, AB Keen, JK Ridley, JM Edwards, and CM Harris. A sensitivity study of the sea ice simulation in the global coupled climate model, hadgem3. *Ocean Modelling*, 74:60–76, 2014.

[95] Pierre Rampal, Sylvain Bouillon, Einar Ólason, and Mathieu Morlighem. nextsim: a new lagrangian sea ice model. *The Cryosphere*, 10(3):1055–1073, 2016.

[96] Patrick J Roache. Code verification by the method of manufactured solutions. *J. Fluids Eng.*, 124(1):4–10, 2002.

[97] A. R. Robinson, P. F. J. Lermusiaux, and N. Q. Sloan III. Data assimilation. In Kenneth H. Brink and Allan R. Robinson, editors, *The Global Coastal Ocean-Processes and Methods*, volume 10 of *The Sea*, chapter 20, pages 541–594. John Wiley and Sons, New York, 1998.

[98] Bert Rudels, Hans J Friedrich, Dagmar Hainbucher, and Gerrit Lohmann. On the parameterisation of oceanic sensible heat loss to the atmosphere and to ice in an ice-covered mixed layer in winter. *Deep Sea Research Part II: Topical Studies in Oceanography*, 46(6-7):1385–1425, 1999.

[99] Tony Ryu, Wael Hajj Ali, Patrick J. Haley, Jr., Chris Mirabito, Aaron Charous, and Pierre F. J. Lermusiaux. Incremental low-rank dynamic mode decomposition model for efficient dynamic forecast dissemination and onboard forecasting. In *OCEANS 2022 IEEE/MTS*, pages 1–8, Hampton Roads, VA, October 2022. IEEE.

[100] Tony Ryu, Jacob P. Heuss, Patrick J. Haley, Jr., Chris Mirabito, Emanuel Coelho, Paul Hursky, Martha C. Schönau, Kevin Heaney, and Pierre F. J. Lermusiaux. Adaptive stochastic reduced order modeling for autonomous ocean platforms. In *OCEANS 2021 IEEE/MTS*, pages 1–9. IEEE, September 2021.

[101] T. P. Sapsis. *Dynamically Orthogonal Field Equations for Stochastic Fluid Flows and Particle Dynamics*. PhD thesis, Massachusetts Institute of Technology, Department of Mechanical Engineering, Cambridge, MA, February 2011.

[102] Themistoklis P. Sapsis and Pierre F. J. Lermusiaux. Dynamically orthogonal field equations for continuous stochastic dynamical systems. *Physica D: Nonlinear Phenomena*, 238(23–24):2347–2360, December 2009.

[103] Themistoklis P. Sapsis and Pierre F. J. Lermusiaux. Dynamical criteria for the evolution of the stochastic dimensionality in flows with uncertainty. *Physica D: Nonlinear Phenomena*, 241(1):60–76, 2012.

[104] Jörg Schröder, Carina Nisters, and Tim Ricken. On a least-squares finite element formulation for sea ice dynamics. *PAMM*, 18(1):e201800156, 2018.

[105] Carina Schwarz and Jörg Schröder. Simulating sea ice drift in the southern ocean incorporating real wind data using the lsfem. *PAMM*, 21(1):e202100130, 2021.

[106] Clint Seinen and Boualem Khouider. Improving the jacobian free newton–krylov method for the viscous–plastic sea ice momentum equation. *Physica D: Nonlinear Phenomena*, 376:78–93, 2018.

[107] Frank Smith, Alexander Korobkin, Emilian Parau, Daniel Feltham, and Vernon Squire. Modelling of sea-ice phenomena, 2018.

[108] T. Sondergaard and P. F. J. Lermusiaux. Data assimilation with Gaussian Mixture Models using the Dynamically Orthogonal field equations. Part I: Theory and scheme. *Monthly Weather Review*, 141(6):1737–1760, 2013.

[109] T. Sondergaard and P. F. J. Lermusiaux. Data assimilation with Gaussian Mixture Models using the Dynamically Orthogonal field equations. Part II: Applications. *Monthly Weather Review*, 141(6):1761–1785, 2013.

[110] Scott R Stephenson and Rebecca Pincus. Challenges of sea-ice prediction for arctic marine policy and planning. *Journal of Borderlands Studies*, 33(2):255–272, 2018.

[111] D. N. Subramani, P. J. Haley, Jr., and P. F. J. Lermusiaux. Energy-optimal path planning in the coastal ocean. *Journal of Geophysical Research: Oceans*, 122:3981–4003, 2017.

[112] D. N. Subramani and P. F. J. Lermusiaux. Energy-optimal path planning by stochastic dynamically orthogonal level-set optimization. *Ocean Modeling*, 100:57–77, 2016.

[113] Deepak Subramani and Pierre F. J. Lermusiaux. Probabilistic ocean predictions with dynamically-orthogonal primitive equations. In preparation, 2023.

[114] Deepak N. Subramani and Pierre F. J. Lermusiaux. Risk-optimal path planning in stochastic dynamic environments. *Computer Methods in Applied Mechanics and Engineering*, 353:391–415, August 2019.

[115] Deepak Narayanan Subramani. *Probabilistic Regional Ocean Predictions: Stochastic Fields and Optimal Planning*. PhD thesis, Massachusetts Institute of Technology, Department of Mechanical Engineering, Cambridge, Massachusetts, February 2018.

[116] M. P. Ueckermann and P. F. J. Lermusiaux. 2.29 Finite Volume MATLAB Framework Documentation. MSEAS Report 14, Department of Mechanical Engineering, Massachusetts Institute of Technology, Cambridge, MA, 2012.

[117] M. P. Ueckermann, P. F. J. Lermusiaux, and T. P. Sapsis. Numerical schemes for dynamically orthogonal equations of stochastic fluid and ocean flows. *Journal of Computational Physics*, 233:272–294, January 2013.

[118] Mischa Ungermann and Martin Losch. An observationally based evaluation of subgrid scale ice thickness distributions simulated in a large-scale sea ice-ocean model of the arctic ocean. *Journal of Geophysical Research: Oceans*, 123(11):8052–8067, 2018.

[119] Petteri Uotila, Siobhan OâFarrell, Simon J Marsland, and Dave Bi. A sea-ice sensitivity study with a global ocean-ice model. *Ocean Modelling*, 51:1–18, 2012.

[120] Jorge R Urrego-Blanco, Nathan M Urban, Elizabeth C Hunke, Adrian K Turner, and Nicole Jeffery. Uncertainty quantification and global sensitivity analysis of the los alamos sea ice model. *Journal of Geophysical Research: Oceans*, 121(4):2709–2732, 2016.

[121] Timo Vihma. Effects of arctic sea ice decline on weather and climate: A review. *Surveys in Geophysics*, 35:1175–1214, 2014.

[122] NE Wayand, CM Bitz, and E Blanchard-Wrigglesworth. A year-round subseasonal-to-seasonal sea ice prediction portal. *Geophysical Research Letters*, 46(6):3298–3307, 2019.

[123] Dongbin Xiu and George Em Karniadakis. Modeling uncertainty in flow simulations via generalized polynomial chaos. *Journal of computational physics*, 187(1):137–167, 2003.

[124] Jinlun Zhang and WD Hibler III. On an efficient numerical method for modeling sea ice dynamics. *Journal of Geophysical Research: Oceans*, 102(C4):8691–8702, 1997.

[125] Jinlun Zhang and DA Rothrock. Effect of sea ice rheology in numerical investigations of climate. *Journal of Geophysical Research: Oceans*, 110(C8), 2005.